DIGITAL ACCESS TO SCHOLARSHIP AT HARVARD
DASH.HARVARD.EDU

HARVARD LIBRARY

Glucocorticoid Compounds Modify Smoothened Localization and Hedgehog Pathway Activity

Citation

Wang, Yu, Lance Davidow, Anthony C. Arvanites, Joel Blanchard, Kelvin Lam, Ke Xu, Vatsal Oza et al. 2012. Glucocorticoid compounds modify smoothened localization and hedgehog pathway activity. Chemistry & Biology 19(8): 972-982.

Published version

https://doi.org/10.1016/j.chembiol.2012.06.012

Link

http://nrs.harvard.edu/urn-3:HUL.InstRepos:9555244

Terms of use

This article was downloaded from Harvard University's DASH repository, and is made available under the terms and conditions applicable to Open Access Policy Articles (OAP), as set forth at
https://harvardwiki.atlassian.net/wiki/external/NGY5NDE4ZjgzNTc5NDQzMGIzZWZhMGFlOWI2M2EwYTg

Accessibility

https://accessibility.huit.harvard.edu/digital-accessibility-policy

Share Your Story

The Harvard community has made this article openly available.
Please share how this access benefits you. Submit a story

Glucocorticoid Compounds Modify Smoothened Localization and Hedgehog Pathway Activity

Yu Wang [1,2,4,7], Lance Davidow[1,3], Anthony C. Arvanites [1,3], Joel Blanchard[1,3,8], Kelvin Lam[1,3,9], Ke Xu[1,3], Vatsal Oza[1,3], Jin Woo Yoo[5], Jessica M.Y. Ng[6], Tom Curran[6], Lee L. Rubin[1,3,10], Andrew P. McMahon[1,2,3,10].

1. Department of Stem Cell and Regenerative Biology,

2. Department of Molecular and Cellular Biology

3. Harvard Stem Cell Institute

4. Department of Chemistry and Chemical Biology

5. Harvard College

Harvard University

Cambridge, MA 02138

6. Children's Hospital of Philadelphia,

Philadelphia, PA 19104

7. Current address: The Morgridge Institute for Research, Madison, WI 53706

8. Current address: The Scripps Research Institute, La Jolla, CA 92037

9. Current address: Blue Sky Biotech, Inc., Worcester, MA 01605.

10. Corresponding authors:

Andrew McMahon

Tel: 617 496 3757 Fax: 617 496 3763

Email: amcmahon@mcb.harvard.edu

and

Lee Rubin

Tel: 617 384 8105 Fax: 617 495 3961

Email: lee_rubin@harvard.edu

Running Title: Glucocorticoid Crosstalk with Hedgehog Signaling

Summary

The Hedgehog signaling pathway is linked to a variety of diseases, notably a range of cancers. The first generation of drug screens identified Smoothened (Smo), a membrane protein essential for signaling, as an attractive drug target. Smo localizes to the primary cilium upon pathway activation, and this transition is critical for the response to Hedgehog ligands. In a high content screen directly monitoring Smo distribution in Hedgehog responsive cells, we identified different glucocorticoids as specific modulators of Smo ciliary accumulation. One class promoted Smo accumulation, conferring cellular hypersensitivity to Hedgehog stimulation. In contrast, a second class inhibited Smo ciliary localization and signaling activity by both wildtype Smo, and mutant forms of Smo, SmoM2 and SmoD473H, that are refractory to previously identified Smo antagonists. These findings point to the potential for developing glucocorticoid-based pharmacological modulation of Smo signaling to treat mutated drug-resistant forms of Smo, an emerging problem in long-term cancer therapy. They also raise a concern about potential crosstalk of glucocorticoid drugs in the Hedgehog pathway, if therapeutic administration exceeds levels associated with on-target transcriptional mechanisms of glucocorticoid action.

Glucocorticoids——graphical abstract

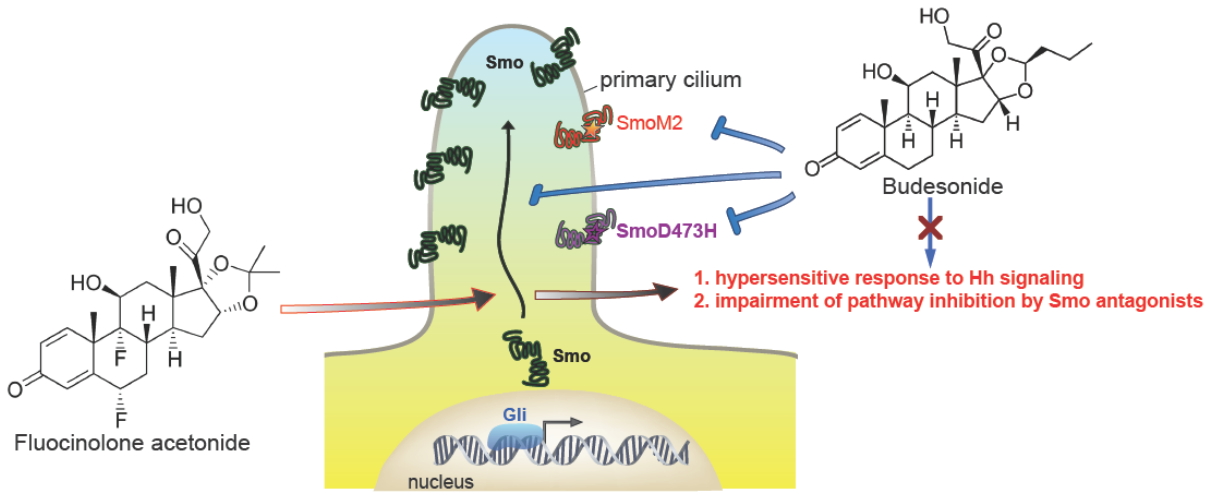

Highlights

- Screened 5,672 compounds from annotated compound libraries for their ability to modulate Smo movement to the primary cilium
- Identified a large class of glucocorticoids such as fluocinolone acetonide (FA) that have the unusual property of promoting Smo accumulation in the primary cilium, whilst not substantially activating a transcriptional response – a chemical separation of what are likely distinct mechanisms of Smo activation
- Demonstrated that these compounds sensitize cells to Hh input
- Provided evidence that high dose off target effects of glucocorticoids can potentially modify the efficacy of current pathway antagonists in clinical trials for anti-cancer activities
- Extended SAR on glucocorticoid scaffold identifies pathway inhibitors, which, importantly, show equal efficacy in inhibiting Smo mutant forms resistant to current therapeutic lead compounds

E-TOC Paragraph

Using a new high content screen, a number of glucocorticoid drugs were identified promoting translocation of Smoothened to the primary cilium, a cell organelle where Hedgehog signaling occurs. Selective characterization of potent hits discovered such glucorticoids lead to sensitized cell response to Hedgehog input and less effective inhibition by Smo antagonists. Further, an extended study of structure-activity relationship identified Budesonide as an antagonist of Smoothened ciliary translocation, which displayed equal efficacy in inhibiting wildtype and mutant Smoothened that are refractory to current therapeutic lead compounds.

Introduction

The Hedgehog (Hh) pathway is one of the central pathways of animal development, and deregulated pathway activity underlies a multitude of diseases, notably a variety of cancers (Rubin and de Sauvage, 2006). Activating mutations in Hh pathway components are cell intrinsic causal factors in cancers linked to Gorlin syndrome, medulloblastoma (MB), basal cell carcinoma (BCC), and rhabdomyosarcoma (RMS). In addition, paracrine Hh signaling-based modulation of the tumor microenvironment is thought to play a wider role in the support of a number of other malignancies including those of the breast, lung, liver, stomach, pancreas, prostate, and colon (Yauch, et al., 2008). Hh signaling is also linked to medically beneficial actions such as the promotion of stem/progenitor cell proliferation that may enable regenerative

therapies. Considerable clinical interest has developed about the mechanisms of Hh pathway action and the identification of drugs that can modulate pathway activity.

Smoothened (Smo), a seven-pass transmembrane protein, has emerged as a predominant target in screens for small-molecule pathway modulators. Smo is essential for all Hh signaling(Zhang, et al., 2001). All 7 drugs in clinical trials for Hh targeted cancer therapy act directly on Smo to inhibit Hh signaling(Tremblay, et al., 2010). Among these, GDC0449 (also known as RG3616 or Vismodegib), was recently approved by the US Food and Drug Administration(FDA) for indication of advanced BBC(Allison, 2012). On the other hand, it was reported that administration of at least two clinical Smo antagonists (GDC0449 and LDE225) resulted in cancer relapse in human and/or mouse in part due to emergence of drug resistant mutations of Smo, which highlighted an unmet medical need for next generation Smo antagonists that can circumvent such mutations (Buonamici, et al., 2010; Yauch, et al., 2009). Smo regulation is quite unusual. Hh binding to its receptor Patched-1 (Ptch1) counters Ptch1 mediated inhibition of Smo, enabling Smo-dependent activation of a Gli-based transcriptional response (Rohatgi, et al., 2007). These events correlate with, and are critically linked to, the primary cilium (PC), a tubulin-based cell extension present on most vertebrate cells(Goetz and Anderson, 2010).After binding Hh, Ptch1 moves from the PC while Smo accumulates on the ciliary axoneme. Though the mechanistic details are unclear, Smo action at the PC is essential for pathway activation(Han, et al., 2009; Wong, et al., 2009), and this cellular translocation presents an opportunity for novel drug development**.**

Here we report on a high content screen (HCS) to identify small molecules that modulate Smo accumulation at the PC. Most strikingly, we identified a large number of glucocorticoids (GC), several of which are in clinical use, that induce this activity. Surprisingly, these compounds fail

to trigger robust pathway activation; instead, they sensitize cells to Hh ligand input and impair pathway inhibition by co-administered pharmacological antagonists of Smo signaling. In contrast, anther steroid, Budesonide , inhibits Smo ciliary translocation and Hh signaling, synergizing with GDC0449, a Smo antagonist under clinical evaluation. Importantly, Budesonide acts similarly on wildtype Smo, and mutant forms refractory to other Smo antagonists, SmoM2 and SmoD473H (Xie, et al., 1998; Yauch, et al., 2009). These findings have important ramifications for the design of new therapeutic approaches to treat cancers whose growth can be modulated by Smo activation, and potential implications for off-target crosstalk of glucocorticoid drugs in the Hedgehog signaling pathway.

Results

Development of a high content screen to identify agonists of Smo ciliary accumulation.

To gain a more comprehensive view of the Hh pathway at early stages of drug development, we developed and validated a novel High Content Screening (HCS) method based directly on Smo translocation to the PC(Wang, et al., 2012). Herein we report our findings while using the method to identify agonists of Smo ciliary accumulation. An EGFP tagged form of human Smo was introduced into Hh responsive NIH3T3 cells(Wang, et al., 2009) (Fig. S1 A) to generate a clonal cell line in which Hh-dependent accumulation of Smo::EGFP in the PC mirrored movement of endogenous Smo(Wang, et al., 2009). An Inversin(Ivs)::tagRFPT expression cassette provided a constitutive, independent PC marker (Watanabe, et al., 2003).

Custom algorithms were developed to perform quantitative multi-parametric image analyses(Wang, et al., 2012). Robust dose dependent responses were observed upon treatment with several known small molecule modulators of Smo: the agonist SAG and the antagonist

cyclopamine (Cyc), both of which directly bind Smo, and forskolin (FKL), whose stimulatory action on protein kinase A inhibits Smo signaling (Fig. S1 A-F). Despite the fact that Cyc and SAG physically interact with Smo in a competitive fashion suggesting a common binding mechanism, and that both induce ciliary accumulation, Cyc bound Smo is inactive. Thus, accumulation within the primary cilium appears to be essential but not sufficient for downstream activation of the Hh pathway. In contrast, FKL likely induce Smo ciliary accumulation indirectly potentially by accelerating anterograde intraflagellar transport (Besschetnova, et al., 2010). A better understanding awaits a clearer picture of the cellular trafficking processes. As a demonstration of the assay's ability to detect local changes within the PC, elongation of the PC on FKL treatment was detected as an expanded Ivs+ domain (last panel in Fig. S1 F), consistent with a recent report(Besschetnova, et al., 2010).

Screening results

We conducted a screen with a library consisting of 5,672 compounds with annotated activities, including FDA approved drugs and drug candidates in preclinical or clinical development. Representative examples of plates including small-molecule control wells are shown for the analysis (Fig. S1 G). Z-prime scores(Zhang, et al., 1999) consistently >0.4 indicate a reasonable reliability of the primary screen.

Approximately 60 compounds in 15 distinct chemical classes were confirmed to induce Smo accumulation at the PC, after rigorous assessment of the dose-response curves for primary hits. As expected, these comprised both pathway agonists and antagonists. For example, LY 294002, an inhibitor of phosphatidylinositol 3-kinase (PI3K) (Vlahos, et al., 1994), induces Smo ciliary accumulation, but inhibits Hh signaling (Fig. S1 H-K). The PI3K pathway is important in a

variety of cancer types and may intersect with the Hh pathway in tumorigenesis (Hambardzumyan, et al., 2008). In combination treatment, a PI3K inhibitor and a Smo antagonist delayed the onset of drug resistance in a mouse model of medulloblastoma (Buonamici, et al., 2010; Dijkgraaf, et al., 2011). PI3K action has also been linked to the regulation of Gli proteins through the Akt pathway (Riobo, et al., 2006). These data suggest that PI3K may act at multiple levels in Hh signaling.

Strikingly, the most predominant chemical class identified comprised naturally occurring and synthetic glucocorticoids (GC), several of which are widely used as anti-inflammatory agents in the clinic (Fig. 1 A-B; Fig. S1 L) (Sommer and Ray, 2008). Interestingly, a recent screen examining β-arrestin aggregation identified an overlap with a subset of these compounds, lending additional support to a GC intersection in Smo-directed Hedgehog signaling, but also raising the possibility of alternative mechanisms (Wang, et al., 2010). Structure-activity relationship (SAR) analysis suggests that fluorine at position 9, a ketal at positions 16 and 17, and protonation at position 11 significantly enhance the potency of this class of compounds in directing Smo accumulation to the PC (Fig. 1 C).

GCs accumulate Smo in the PC without activating the Hh pathway.

To investigate in more detail the consequences of GC-induced Smo accumulation in the PC, and to obtain mechanistic insights into GC action in the Hh pathway, we first chose one compound in clinical use, fluocinolone acetonide (FA). FA displays an EC50 of around 5 μM for accumulation of Smo in the PC; in addition, no obvious cytotoxic effects are observed *in vitro* at much higher doses (up to 200 μM; Fig. 1 B and D, Fig. S1 M). Localization of an inversin-based PC reporter and other PC markers including Arl13b, acetylated tubulin, and detyrosinated α-

tubulin (glu-tub) were unaltered in response to FA (Fig. 1D; Fig. S1 M and N)(Caspary, et al., 2007; Schroder, et al., 2007; Watanabe, et al., 2003). Further, no change was detected in the activity of a Wnt-signaling reporter in response to FA concentrations that modify Smo distribution (Fig. S1 O). Together these data suggest that FA's effects in this assay are specific to the Hh pathway.

The accumulation of Smo in the PC is thought to be essential for transcriptional activation of the Hh pathway (Kim, et al., 2009; Rohatgi, et al., 2007). However, we observed a marked disparity between FA-induced Smo accumulation in the PC and Hh pathway activation in transcription reporter assays. At low levels of FA that effectively promote Smo accumulation in the PC (10 μM), no pathway activation was observed. Higher concentrations (>50 μM) invoked a weak transcriptional response measurable in a Gli-luciferase reporter assay (4 fold versus 25 fold for 1 μM of the Smo agonist SAG in the same assay (data not shown)), and on quantitative reverse transcription–polymerase chain reaction (qRT-PCR) measurement of Hedgehog target gene expression (*Ptch1* and *Gli1*; Fig. 2A-B). The EC50 for weak transcriptional activation (>50 μM) was 10 fold higher than that of FA-induced accumulation of Smo within the PC.

FA induces hypersensitivity to Hh pathway stimulation.

The effects of FA resemble over-expression of Smo in that constitutive accumulation of wild-type Smo within the PC only results in weak pathway activation (Fig. S2 A). Ciliary accumulation of Smo sensitizes cells to subsequent Sonic hedgehog (Shh) ligand input, raising the possibility that FA-driven Smo accumulation may sensitize Hh responsive cells. Indeed, co-stimulation of cells with 10 μM FA results in a dose-dependent enhancement of a Shh-induced transcriptional response (Fig. 2 C-D). Furthermore, this effect was measurable after prolonged withdrawal of FA; cells treated for 24 hours with FA followed by compound withdrawal prior to

Shh addition showed a higher induction of pathway activity than DMSO treated controls (Fig. 2 E-F). The EC50 of a FA induced response to priming is approximately 4 μM, in good agreement with the dose required for efficient accumulation of Smo in the PC (Fig. 1 B). Smo turnover in the PC is relatively slow after Shh-invoked pathway activation(Wang, et al., 2009), or compound withdrawal (Fig. S2 B-C), providing a potential explanation for a FA induced pathway priming effect. FA treatment showed no effect on Wnt pathway activity (Fig. S1 O), consistent with Hh pathway specificity.

FA may regulate Smo by direct binding.

To determine whether FA interacts with Smo, we performed a competition assay with Bodipy-Cyc. Cyc binds Smo directly (Chen, et al., 2002) and its fluorescent analog, Bodipy-Cyc, shows strong Smo-dependent fluorescence within cells over-producing Smo (identified by co-expression of a nuclear localized tagRFP-T, Fig. 2 G-H). An oncogenic mutation within the 7th transmembrane domain (SmoM2, also named SmoA1, Fig. 2 H-I) (Chen, et al., 2002), and a recently described drug resistance mutation within the 6th transmembrane domain (SMOD473H) significantly impair Cyc binding to Smo, suggesting that these are critical sites for chemical interaction (Yauch, et al., 2009).

FA displayed a dose-dependent competition of Bodipy-Cyc binding to wild-type Smo, similar to other small molecules that directly bind Smo (SAG, and GDC0449), or that likely interact directly with Smo based on similar competition assays (SANT-1) (Fig.2 H-I) (Chen, et al., 2002; Chen, et al., 2002; Frank-Kamenetsky, et al., 2002; Yauch, et al., 2009). In contrast, FKL induces Smo accumulation in the PC but does not compete with Bodipy-Cyc, reflecting an indirect action through its protein kinase A target (Milenkovic, et al., 2009; Wilson, et al., 2009).

Weak pathway activation induced by FA was attenuated by Smo antagonists (Fig. 2 A) and depended on endogenous Smo as activation was not observed in fibroblasts lacking Smo activity (Fig.S2D). SANT-1 and GDC0449 inhibit FA promoted accumulation of Smo in the PC (Fig. S2 E-F). Collectively, these data support a direct interaction between FA and Smo.

Antagonistic drug-drug interactions between FA and Smo antagonists

Considering that GCs and various Hh pathway antagonists may share a common Smo target, and GCs are widely used to suppress inflammation in conjunction with cancer therapy, we next asked whether we could observe a potential GC crosstalk with Smo antagonists in cell culture assays. Hh pathway inhibition by GDC0449, Cyc and SANT-1, as measured by both Gli-luciferase induction (Fig. 3A and Fig. S3) and Smo ciliary localization (Fig.3 B-C and Fig. S3), was dramatically reduced *in vitro* in the presence of FA. Thus, FA co-treatment leads to a drug-dependent alteration of cellular response to chemical inhibitors of Smo. This may occur through competition, or the requirement for a higher level of GDC-0449 to inhibit Hh-driven pathway activity in the presence of GC, but the outcome resembles the genetic resistance seen with a dominant active Smo mutation (SmoM2) (Fig. 3A).

Common properties of FA and TA in modulating Smo localization and Hh pathway activity.

We next assessed whether the observations for FA were replicated by a second clinically approved GC, Triamcinolone Acetonide (TA). TA was slightly more potent than FA in Smo ciliary translocation assay (Fig.1B). Similar to FA, TA only evoked a Gli-mediated transcriptional response at much higher doses than those that induced Smo ciliary accumulation, although the Hh pathway was activated to higher levels than measured on FA treatment

(Fig.S4A). No activation was observed in Smo-/- embryonic fibroblast cells as expected (Fig.S2D). Further, at 10 μM TA enhanced the response to Hh ligand (Fig.S4B), a dose that does not sufficient to induce ligand-independent pathway activity (Fig.S4A). TA also displayed a dose dependent competition with Bodipy-Cyc for binding to Smo (Fig.S4C-D). More importantly, 10 μM TA induced a dose-response shift for GDC0449 mediated inhibition of Hh pathway activity, and Smo ciliary accumulation induced by ligand treatment (Fig. S4E-G). Taken together, our results indicate that these, and possibly other GCs that alter Smo localization share broadly similar biological properties but further work will be required to examine the extensive set of compounds identified in our study.

<u>*ex vivo* studies of FA with Ptch1+/- CGNPs</u>

To further explore FA actions, we isolated cerebellar granule neuron precursors (CGNPs) from Ptch1+/- neonates. Proliferation of CGNP is Shh-dependent and *Ptch1* heterozygosity predisposes both mice and humans to develop CGNP-derived medulloblastoma (Schuller, et al., 2008). Consistent with results on Hh pathway activation in NIH3T3 cells, only very high doses of FA (120 μM) elevated the number of proliferative, phospho-histone H3 (pH3) positive GCNPs (Fig. 4 A-B). However, a lower dose of FA (10 μM) markedly enhanced Shh-driven CGNP proliferation (Fig. 4 C-D). Further, co-administration of FA(10 μM), with the Smo antagonist GDC0449, impaired GDC0449 inhibition of Shh-stimulated GCNP proliferation (Fig. 4 E-F).

<u>GC inhibitors of Smo accumulation to the PC and of Smo signaling.</u>

While a large number of GCs promote Smo ciliary accumulation, secondary assays of small molecules sharing the core GC scaffold identified two inhibitory GCs: Budesonide (Bud) and

Ciclesonide (Cic) (Fig. 5 A-C; Fig. S5 A-C). When compared with Smo promoting GCs, Bud and Cic are distinguished by bulky hydrophobic groups at positions 16 and 17 (Fig. 1; Fig. S1 L; Fig.5A; Fig. S5 A). In contrast to FA and TA, Bud had no pathway inducing activity, nor did Bud induce a hypersensitive response to Hh ligand (Fig. 2 A-F; Fig. 5 D), reinforcing the association of hyper-responsiveness to Smo ciliary accumulation activity. As expected from the inhibition of Smo accumulation in the PC, Bud and Cic inhibited Shh dependent activation of a Gli-reporter (Fig. 5 E and Fig. S5 D). Further, Bud attenuated Smo ciliary accumulation and pathway activation by SAG (Fig. 5 E; Fig. S5 E-F), and also suppressed Cyc induced Smo accumulation to the PC (Fig. S5 E-F). Bud treatment showed no effect on Wnt pathway activity (Fig. S5 G), consistent with a specific modulation of Hh signaling outside of its GC activity.

Bud inhibits ciliary localization and signaling of drug resistant mutants of Smo.

SmoM2 encodes a dominant active Smo variant identified in a human cancer that is resistant to inhibition by available Smo antagonists at concentrations that completely suppressed wildtype Smo activity (Fig. S5 H-K)(Xie, et al., 1998). Unexpectedly, both Bud and Cic attenuated SmoM2 ciliary localization, and downstream pathway activity, as effectively as wildtype Smo (Fig. 5 F-H; Fig. S5 L-M). Bud and Cic did not disrupt ciliary structure or ciliary trafficking: acetylated-tubulin (acet-tub), Ivs::tagRFPT, and Arl13b::tagRFPT within the PC were unaltered on treatment (Fig. S5 N-R).

The emergence of a drug resistant form of Smo with a D473H mutation was reported in a MB patient during treatment with GDC0449. The appearance of this mutation associated with a re-emergence of the tumor (Yauch, et al., 2009). This finding has triggered a search for antagonists that effectively inhibit the activity of both wildtype and mutant forms of Smo (Dijkgraaf, et al.,

2011; Kim, et al., 2010; Tao, et al., 2011). We examined Bud and GDC0449 in parallel for their inhibition of Hh induced SmoD473H activity, and the corresponding ciliary localization. Smo-/- MEF cells were transfected independently with wildtype and D473H mutant forms of Smo. Both forms rescued the cell's response to Hh ligand (Fig.S5S). As expected, the D473H mutation conferred a dramatic resistance to GDC0449's inhibitory action on both Hh pathway activity and Smo ciliary localization (Fig. S5T-V). In contrast, Bud showed similar efficacies in inhibiting wildtype Smo and SmoD473H activity in both assays (Fig.5I-K).

To examine the site of Bud action in the Hh pathway, we examined Hh signaling activity following removal of suppressor of Fused (suFU) activity, a Gli repressor functioning downstream of Smo. Distinct from GANT61(Lauth, et al., 2007), Bud failed to suppress ligand-independent Hh pathway activity induced by loss of suFU function (Fig. 5L). Together these data suggest that Bud may act at the level of Smo but through a different mechanism than other Smo-interacting antagonists including SANT-1, Cyc, and GDC0449, and also distinct from FA and SAG. Consistent with a unique inhibitory action, Bud failed to compete with Bodipy-Cyc even at levels well above the inhibitory maximum (100 μM; Fig. 5 M-N). Further, whereas FA competed with GDC0449 to suppress effective pathway inhibition (Fig. 3), Bud enhanced GDC0449's activity to block Smo accumulation at the PC and Hh pathway inhibition (Fig. 6).

Discussion

The interaction of GCs with the Hh pathway leads to several important observations: First, all small molecules that induce ligand-independent Smo accumulation to the PC characterized to date either activate or inhibit Smo activity. Agonists include SAG and purmorphamine (Chen, et al., 2002; Frank-Kamenetsky, et al., 2002; Sinha and Chen, 2006). Cyc though an antagonist also

induces Smo transolcation to the PC(Rohatgi, et al., 2009; Wang, et al., 2009; Wilson, et al., 2009). Several lines of evidence indicate that whereas Smo accumulation in the PC is essential for signaling, accumulation is not sufficient, with additional ligand-dependent actions being required to generate an active form of Smo (Rohatgi, et al., 2009; Wang, et al., 2009; Watanabe, et al., 2003; Wilson, et al., 2009). Together, our data suggest that many GCs can function in a novel mechanism that synergizes with Hh-ligand-directed signaling by promoting accumulation of Smo within the primary cilium. The synergistic effect might result from bypassing a Ptch1-mediated "barrier" for Smo entry to the primary cilium facilitating the activation of Smo, which appears to be restricted to this organelle. The mechanism of divergent pharmacological modulations of Smo ciliary translocation and its activity is not understood. A recent report suggested that Smo phosphorylation plays a role in its ciliary translocation and activation (Chen, et al., 2011). Further study of small molecule directed changes in Smo phosphorylation will enhance our understanding of the significance of phosphorylation in localization and activity.

Second, the finding of a potential effect of Smo promoting GCs in modulating the Hh response highlights the value of a “direct target screen” focusing on critical parameters of target action. To date most small molecule Hh pathway modulators have been identified through “end-point” transcriptional assays. However, because of their modest effects on transcription, GC interactions are not readily detected with this screening approach. Such disparity suggests that the mechanism of pharmacological induction of Smo accumulation to the primary cilium and its retention there is divergent from that of its activation.

Third, the dose of GC required to modify Smo localization (EC50s>1 μM) is significantly higher than that required to directly modulate GC receptor-based transcriptional responses (EC50s <10 nM or lower (Johnson, 1998)). Thus, we believe GC’s likely act directly on Smo at

high concentrations, and not indirectly through a nuclear hormone receptor triggered transcriptional regulatory action.

Fourth, naturally occurring hydrocortisone and cortisone show different potencies in accumulating Smo to the PC (Fig. 1 A and B). 11β-hydroxysteroid dehydrogenase type 2 (HSD11β2), an enzyme that transforms hydrocortisone into cortisone, is up-regulated by Hh signaling in CGNPs (Heine and Rowitch, 2009), whereas HSD11β1, an enzyme that mainly catalyzes the reverse reaction, was recently discovered as a target gene for Hh signaling in prostate cancer tissue (Shaw, et al., 2009). Taken together, these findings suggest potential feedback mechanisms linking the Hh transcriptional output to steroid regulation of Smo action.

Fifth, inflammation and cancer are linked, necessitating combinatorial therapies to treat both aspects of disease (Mantovani, et al., 2008). To this end, GCs are frequently co-administered to patients receiving anti-cancer therapies. However, GCs are reported to enhance cancers of the breast (Sui, et al., 2006), colon (Zhang, et al., 2006), lung (Herr, et al., 2003), ovary (Sui, et al., 2006; Zhang, et al., 2006), and pancreas (Zhang, et al., 2006), and to increase the metastatic potential of breast cancer (Sherlock and Hartmann, 1962). Amongst these are glucocorticoids that promote Smo ciliary accumulation in the current study. Further, FA is reported to act as a tumor promoter in the skin(Fukao, et al., 1988). Our studies also raise the possibility of high dosing of glucocorticoids leading to off-target action of glucocorticoid agents in the Hh pathway, modifying therapeutic outcome: for example, in Hh-antagonist-directed cancer therapy. Whether an effective dose for GC drug-mediated crosstalk is reached during therapeutic administration is not clear, but the pharmacokinetics of certain GC drugs in human patients may warrant further investigation. For example, a peak plasma concentration of Dexamethasone, a broadly used GC in cancer patients, has been reported at >10 μM after a single high dose (Brady, et al., 1987),

which falls in the range where significant Smo cilial accumulation occurs in vitro (data not shown). Long-term systematic treatment, common in cancer therapy, might result in longer exposure to higher concentrations. Further, high dose of glucocorticoids are given to preterm infants to accelerate maturation of the lungs. Whether glucocorticoids in this scenario may influence developmental Hh signaling is not known.

Sixth, our data suggest that most GCs likely share a similar interaction site with a broad range of agonists and antagonists including SAG, GDC0449, SANT-1, and Cyc, or modify Smo on binding to block access to this binding region. In contrast, Bud-like GCs do not compete with other Smo antagonists. Further, Bud works equally well inhibiting wildtype Smo and mutant forms of Smo refractory to clinically active inhibitory compounds. Thus, it may act more like an allosteric regulator of Smo activity. Interestingly, GDC0449 resistant SmoD473H can be readily inhibited by it's the related benzimidazole HhAntag (Dijkgraaf, et al., 2011). Subsequent efforts to improve Bud potency should keep in mind the clinical imperative of pan-inhibition of Smo mutant forms. Collectively, our findings highlight the potential to develop new drugs around a GC scaffold that may synergize with compounds currently undergoing clinical development to enhance anti-Hh-based cancer therapies and may also reveal more about the ways in which Smo trafficking and activity are regulated.

Acknowledgements

We are very grateful to C. T. Walsh, S.L. Schreiber, and A. Saghatelian for critical review of our results and helpful discussions. We thank J.W. Lichtman, R.Y. Tsien, M.P. Scott, and P.T. Chuang for sharing reagents. We thank R. A. Segal and X. Zhao for technical assistance on

CNGP cell culture and our colleagues in the McMahon and Rubin laboratories for support on our research. We also thank Dr. James A. Thomson for his support. This work was funded by the Harvard Stem Cell Institute (DP-0033-08-02 to A.P.M and L.L.R) and National Institutes of Health (R37 NS033642 to A.P.M). Y.W, L.L.R and A.P.M hold patent positions around Hedgehog signaling and drug discovery platforms. Intellectual property protection is being developed about the assay and compounds herein.

Author Contributions

Y. W, L.L.R and A.P.M conceived the project. Y. W. developed and validated the assay. Primary screens and secondary assays and data analysis were performed by Y.W, J.B, L. D, A. A, K. L., J. W. Y., J.M.N and T.C.. Y.W., L.L.R., and A.P.M. wrote the paper.

Materials and Methods

Cell Culture

NIH/3T3 cells were maintained in DMEM containing 10%(v/v) calf serum, penicillin, streptomycin, and L-glutamine. HEK293, L, cos7 , and suFU-/- mouse embryonic fibroblast cells were maintained in DMEM containing 10%(v/v) fetal bovine serum, penicillin, streptomycin, and L-glutamine. Smo::EGFP and Ivs:: tagRFPT were cloned into pBabe retroviral constructs. Smo::EGFP/Ivs::tagRFPT stable cell lines was generated through viral infecting NIH/3T3 cells according to the procedure described previously(Wang, et al., 2009). A ShhLightII cell line (ATCC) was used for Gli-luciferase reporter assays. This line contains a stably integrated Gli-responsive firefly luciferase reporter and a constitutive *Renilla* luciferase expression construct (Taipale, et al., 2000). A subclone of this cell line was created expressing a stably integrated

SmoM2 expression construct. Shh conditioned medium was collected from cos7 cells transfected with an expression construct encoding the amino terminal 19kDa signaling peptide of Shh and used at 13.7(±3.0)nM unless stated otherwise. Control conditioned medium was collected from cos7 cells transfected with an empty plasmid. Wnt3a conditioned medium was collected from an L cell line stably expressing a Wnt3a expression construct. Control conditioned medium was collected from wild-type L cells. All conditioned medium were diluted 1:10 prior to assay.

Reagents

Chemical libraries screening utilized the Library of Pharmacologically Active Compounds (LOPAC, Sigma-Aldrich), the Spectrum Collection (Microsource Discovery Systems), and the Prestwick Chemical Library (Prestwick Chemical), along with a custom collection of additional biologically annotated chemistries absent from the above pre-plated reference collections. Glucocorticoids, cyclopamine, forskolin, mouse monoclonal anti-acetylated tubulin antibody for follow-up studies were purchased from Sigma. SAG was purchased from Axxora Platform. SANT-1 was obtained from Tocris Biosciences. GDC0449 was purchased from Selleck Chemicals. BODIPY-cyclopamine was purchased from Toronto Research Chemicals. All small molecule stock solutions were prepared by dissolving in DMSO at 1 or 10 mM and stored at -20°C. Mouse recombinant ShhN purified protein (IIShhN) was a gift from Dr. Pepinsky (Biogen Inc). Rabbit polyclonal anti-detyrosinated α-tubulin (Glu-tub) was from Chemicon, Mouse monoclonal anti-Arl13b antibody was from Antibody Incorporated. Secondary antibodies were from Life Technologies. Transfection was performed using Fugene6 or Fugene HD (Roche).

Imaging Assays

Cells were cultured and treated in 384-well imaging plate precoated with poly-D-Lysine (Greiner Bio-one) , fixed with 4% paraformaldehyde (Electron Microscopy Sciences) , and

stained with Hoechst(Life Technologies). Immunofluorescence staining was conducted with standard procedures when necessary. Images were collected using Opera High Content Screening System (Perkin Elmer). ActivityBase (IDBS), Pipeline Pilot (Accelrys), Excel (Microsoft), and Prism (GraphPad) were used for high content screening data management and analysis. Acapella 2.0 software (Evotec Technologies/PerkinElmer) was used to perform multi-parametric image quantification. All the comparative images were scanned with identical microscopic setting and analyzed with the same input parameters.

Hh and Wnt activity assays

ShhLightII cells and SmoM2/LightII cells were cultured and treated in 96 well assay plates (Corning) and incubated with Duo-Glo luciferase substrates (Promega) to sequentially measure firefly and renilla luciferase activity. Smo, or GFP, expression plasmids were co-transfected into 3T3 cells together with a Gli-responsive firefly reporter and a TK-renilla luciferase reporter contruct to monitor effects of Smo overexpression. Co-transfection of the two reporter constructs was conducted in assays measuring Hh pathway activity in suFU-/- cells. Wnt activity was measured following co-transfection of a Top-flash and renilla luciferase reporter. In both Hh and Wnt activity assays, renilla luciferase reporter activity, or mass of protein, was used to normalize expression values. Luciferase signal was read by TopCount NX Microplate Scintillation and Luminescence Counter(Perkin Elmer)**.** Quantitative PCR probes for *Ptch1*, *Gli1*, and *β-actin* were purchased from Applied Biosystems. Reactions and measurements were performed using on an Applied Biosystems 7900HT at Harvard FAS Center of System Biology. *β-actin* was used to normalize *Ptch1* and *Gli1* values.

Bodipy-Cyclopamine Competition Assays

Cos7 cells were transfected with a plasmid that co-expresses Smo and a nuclear localized tagRFPT marker (pCIT-Smo). The empty parental construct (pCIT) and a construct that co-express SmoM2 were used as controls to assess specificity and background signal. Three days after transfection, cells were incubated with 5nM Bodipy-cyclopamine, with or without additional compounds, for 1 hour at 37°C. Cells were then fixed and stained with Hoechst. Images were collected with the Opera High Content Screen System. Fluorescence values were assessed in transfected cells (red nuclei) with a program developed by the authors using Acapella 2.0 software. All of images were scanned with identical microscopic setting and analyzed with the same input parameters.

CGNP proliferation Assays

CGNP primary cells were isolated from P7 Ptch1+/- mice as previously reported(Chan, et al., 2009). Cells were seeded in poly-D-lysine coated imaging plates (Greiner Bio-one), treatments were applied 2 hours thereafter and last for 36 hours. Cells then were fixed with 4% paraformaldehyde (Electron Microscopy Sciences) , and stained with anti-pH3 antibody(Upstate; 1:100) followed by a secondary antibody(Invitrogen) and Hoechst(Invitrogen). Images were collected and cell proliferation quantified with a program developed by the authors utilizing Acapella 2.0 software. All of the images in each experiment were collected with identical microscopic settings and analyzed with identical input parameters.

References

Allison, M. (2012). Hedgehog hopes lifted by approval... and stung by failure. Nat Biotechnol 30, 203.
Besschetnova, T.Y., Kolpakova-Hart, E., Guan, Y., Zhou, J., Olsen, B.R., and Shah, J.V. (2010). Identification of signaling pathways regulating primary cilium length and flow-mediated adaptation. Curr Biol 20, 182-187.
Brady, M.E., Sartiano, G.P., Rosenblum, S.L., Zaglama, N.E., and Bauguess, C.T. (1987). The Pharmacokinetics of Single High-Doses of Dexamethasone in Cancer-Patients. Eur J Clin Pharmacol 32, 593-596.

Buonamici, S., Williams, J., Morrissey, M., Wang, A., Guo, R., Vattay, A., Hsiao, K., Yuan, J., Green, J., Ospina, B., et al. (2010). Interfering with resistance to smoothened antagonists by inhibition of the PI3K pathway in medulloblastoma. Sci Transl Med 2, 51ra70.
Caspary, T., Larkins, C.E., and Anderson, K.V. (2007). The graded response to Sonic Hedgehog depends on cilia architecture. Dev Cell 12, 767-778.
Chan, J.A., Balasubramanian, S., Witt, R.M., Nazemi, K.J., Choi, Y., Pazyra-Murphy, M.F., Walsh, C.O., Thompson, M., and Segal, R.A. (2009). Proteoglycan interactions with Sonic Hedgehog specify mitogenic responses. Nature Neuroscience 12, 409-417.
Chen, J.K., Taipale, J., Cooper, M.K., and Beachy, P.A. (2002). Inhibition of Hedgehog signaling by direct binding of cyclopamine to Smoothened. Genes Dev 16, 2743-2748.
Chen, J.K., Taipale, J., Young, K.E., Maiti, T., and Beachy, P.A. (2002). Small molecule modulation of Smoothened activity. Proc Natl Acad Sci USA 99, 14071-14076.
Chen, Y., Sasai, N., Ma, G., Yue, T., Jia, J., Briscoe, J., and Jiang, J. (2011). Sonic Hedgehog dependent phosphorylation by CK1alpha and GRK2 is required for ciliary accumulation and activation of smoothened. PLoS Biol 9, e1001083.
Dijkgraaf, G.J., Alicke, B., Weinmann, L., Januario, T., West, K., Modrusan, Z., Burdick, D., Goldsmith, R., Robarge, K., Sutherlin, D., et al. (2011). Small molecule inhibition of GDC-0449 refractory smoothened mutants and downstream mechanisms of drug resistance. Cancer Res 71, 435-444.
Frank-Kamenetsky, M., Zhang, X.M., Bottega, S., Guicherit, O., Wichterle, H., Dudek, H., Bumcrot, D., Wang, F.Y., Jones, S., Shulok, J., et al. (2002). Small-molecule modulators of Hedgehog signaling: identification and characterization of Smoothened agonists and antagonists. J Biol 1, 10.
Fukao, K., Tanimoto, Y., Kayata, Y., Yoshiga, K., Takada, K., and Okuda, K. (1988). Effects of Fluocinolone Acetonide on Mouse Skin Sterol-Metabolism and 2-Stage Carcinogenesis. Carcinogenesis 9, 1661-1664.
Goetz, S.C., and Anderson, K.V. (2010). The primary cilium: a signalling centre during vertebrate development. Nat Rev Genet 11, 331-344.
Hambardzumyan, D., Becher, O.J., Rosenblum, M.K., Pandolfi, P.P., Manova-Todorova, K., and Holland, E.C. (2008). PI3K pathway regulates survival of cancer stem cells residing in the perivascular niche following radiation in medulloblastoma in vivo. Gene Dev 22, 436-448.
Han, Y., Kim, H., Dlugosz, A., Ellison, D., Gilbertson, R., and Alvarez-Buylla, A. (2009). Dual and opposing roles of primary cilia in medulloblastoma development. Nat Med 15, 1062-1065.
Heine, V.M., and Rowitch, D.H. (2009). Hedgehog signaling has a protective effect in glucocorticoid-induced mouse neonatal brain injury through an 11betaHSD2-dependent mechanism. J Clin Invest 119, 267-277.
Herr, I., Ucur, E., Herzer, K., Okouoyo, S., Ridder, R., Krammer, P.H., Doeberitz, M.V., and Debatin, K.M. (2003). Glucocorticoid cotreatment induces apoptosis resistance toward cancer therapy in carcinomas. Cancer Res 63, 3112-3120.
Johnson, M. (1998). Development of fluticasone propionate and comparison with other inhaled corticosteroids. J Allergy Clin Immunol 101, S434-439.
Kim, J., Kato, M., and Beachy, P. (2009). Gli2 trafficking links Hedgehog-dependent activation of Smoothened in the primary cilium to transcriptional activation in the nucleus. Proc Natl Acad Sci USA 106, 21666-21671.
Kim, J., Lee, J.J., Gardner, D., and Beachy, P.A. (2010). Arsenic antagonizes the Hedgehog pathway by preventing ciliary accumulation and reducing stability of the Gli2 transcriptional effector. Proc Natl Acad Sci U S A 107, 13432-13437.
Lauth, M., Bergström, A., Shimokawa, T., and Toftgård, R. (2007). Inhibition of GLI-mediated transcription and tumor cell growth by small-molecule antagonists. Proc Natl Acad Sci USA 104, 8455-8460.

Mantovani, A., Allavena, P., Sica, A., and Balkwill, F. (2008). Cancer-related inflammation. Nature 454, 436-444.
Milenkovic, L., Scott, M.P., and Rohatgi, R. (2009). Lateral transport of Smoothened from the plasma membrane to the membrane of the cilium. J Cell Biol 187, 365-374.
Riobo, N.A., Lu, K., Ai, X.B., Haines, G.M., and Emerson, C.P. (2006). Phosphoinositide 3-kinase and Akt are essential for Sonic Hedgehog signaling. Proc Natl Acad Sci USA 103, 4505-4510.
Rohatgi, R., Milenkovic, L., Corcoran, R., and Scott, M. (2009). Hedgehog signal transduction by Smoothened: Pharmacologic evidence for a 2-step activation process. Proc Natl Acad Sci USA 106, 3196-3201.
Rohatgi, R., Milenkovic, L., and Scott, M.P. (2007). Patched1 regulates hedgehog signaling at the primary cilium. Science 317, 372-376.
Rubin, L.L., and de Sauvage, F.J. (2006). Targeting the Hedgehog pathway in cancer. Nature Reviews Drug Discovery 5, 1026-1033.
Schroder, J.M., Schneider, L., Christensen, S.T., and Pedersen, L.B. (2007). EB1 is required for primary cilia assembly in fibroblasts. Curr Biol 17, 1134-1139.
Schuller, U., Heine, V.M., Mao, J., Kho, A.T., Dillon, A.K., Han, Y.G., Huillard, E., Sun, T., Ligon, A.H., Qian, Y., et al. (2008). Acquisition of granule neuron precursor identity is a critical determinant of progenitor cell competence to form Shh-induced medulloblastoma. Cancer Cell 14, 123-134.
Shaw, A., Gipp, J., and Bushman, W. (2009). The Sonic Hedgehog pathway stimulates prostate tumor growth by paracrine signaling and recapitulates embryonic gene expression in tumor myofibroblasts. Oncogene 28, 4480-4490.
Sherlock, P., and Hartmann, W.H. (1962). Adrenal Steroids and Pattern of Metastases of Breast Cancer. Jama-J Am Med Assoc 181, 313-317.
Sinha, S., and Chen, J.K. (2006). Purmorphamine activates the Hedgehog pathway by targeting Smoothened. Nat Chem Biol 2, 29-30.
Sommer, P., and Ray, D.W. (2008). Novel therapeutic agents targeting the glucocorticoid receptor for inflammation and cancer. Curr Opin Invest Dr 9, 1070-1077.
Sui, M.H., Chen, F., Chen, Z., and Fan, W.M. (2006). Glucocorticoids interfere with therapeutic efficacy of paclitaxel against human breast and ovarian xenograft tumors. Int J Cancer 119, 712-717.
Taipale, J., Chen, J.K., Cooper, M.K., Wang, B., Mann, R.K., Milenkovic, L., Scott, M.P., and Beachy, P.A. (2000). Effects of oncogenic mutations in Smoothened and Patched can be reversed by cyclopamine. Nature 406, 1005-1009.
Tao, H., Jin, Q., Koo, D.I., Liao, X., Englund, N.P., Wang, Y., Ramamurthy, A., Schultz, P.G., Dorsch, M., Kelleher, J., et al. (2011). Small molecule antagonists in distinct binding modes inhibit drug-resistant mutant of smoothened. Chem Biol 18, 432-437.
Tremblay, M.R., McGovern, K., Read, M.A., and Castro, A.C. (2010). New developments in the discovery of small molecule Hedgehog pathway antagonists. Curr Opin Chem Biol 14, 428-435.
Vlahos, C.J., Matter, W.F., and Brown, R.F. (1994). A Specific Inhibitor of Phosphatidylinositol 3-Kinase. J Cell Biochem, 274-274.
Wang, J., Lu, J., Bond, M.C., Chen, M., Ren, X.R., Lyerly, H.K., Barak, L.S., and Chen, W. (2010). Identification of select glucocorticoids as Smoothened agonists: potential utility for regenerative medicine. Proc Natl Acad Sci U S A 107, 9323-9328.
Wang, Y., Arvanites, A.C., Davidow, L., Blanchard, J., Lam, K., Yoo, J.W., Coy, S., Rubin, L.L., and McMahon, A.P. (2012). Selective Identification of Hedgehog Pathway Antagonists By Direct Analysis of Smoothened Ciliary Translocation. ACS Chem Biol. http://dx.doi.org/10.1021/cb300028a
Wang, Y., Zhou, Z., Walsh, C., and McMahon, A. (2009). Selective translocation of intracellular Smoothened to the primary cilium in response to Hedgehog pathway modulation. Proc Natl Acad Sci USA 106, 2623-2628.

Watanabe, D., Saijoh, Y., Nonaka, S., Sasaki, G., Ikawa, Y., Yokoyama, T., and Hamada, H. (2003). The left-right determinant Inversin is a component of node monocilia and other 9+0 cilia. Development 130, 1725-1734.
Wilson, C.W., Chen, M.-H., and Chuang, P.-T. (2009). Smoothened adopts multiple active and inactive conformations capable of trafficking to the primary cilium. PLoS ONE 4, e5182.
Wong, S., Seol, A., So, P., Ermilov, A., Bichakjian, C., Epstein, E., Dlugosz, A., and Reiter, J. (2009). Primary cilia can both mediate and suppress Hedgehog pathway-dependent tumorigenesis. Nat Med 15, 1055-1061.
Xie, J., Murone, M., Luoh, S.M., Ryan, A., Gu, Q., Zhang, C., Bonifas, J.M., Lam, C.W., Hynes, M., Goddard, A., et al. (1998). Activating Smoothened mutations in sporadic basal-cell carcinoma. Nature 391, 90-92.
Yauch, R., Dijkgraaf, G., Alicke, B., Januario, T., Ahn, C., Holcomb, T., Pujara, K., Stinson, J., Callahan, C., Tang, T., et al. (2009). Smoothened Mutation Confers Resistance to a Hedgehog Pathway Inhibitor in Medulloblastoma. Science 326, 572-574.
Yauch, R.L., Gould, S.E., Scales, S.J., Tang, T., Tian, H., Ahn, C.P., Marshall, D., Fu, L., Januario, T., Kallop, D., et al. (2008). A paracrine requirement for hedgehog signalling in cancer. Nature 455, 406-410.
Zhang, C., Kolb, A., Mattern, J., Gassler, N., Wenger, T., Herzer, K., Debatin, K.M., Buchler, M., Friess, H., Rittgen, W., et al. (2006). Dexamethasone desensitizes hepatocellular and colorectal tumours toward cytotoxic therapy. Cancer Lett 242, 104-111.
Zhang, C.W., Kolb, A., Buchler, P., Cato, A.C.B., Mattern, J., Rittgen, W., Edler, L., Debatin, K.M., Buchler, M.W., Friess, H., et al. (2006). Corticosteroid co-treatment induces resistance to chemotherapy in surgical resections, xenografts and established cell lines of pancreatic cancer. Bmc Cancer 6:61.
Zhang, C.W., Marme, A., Wenger, T., Gutwein, P., Edler, L., Rittgen, W., Debatin, K.M., Altevogt, P., Mattern, J., and Herr, I. (2006). Glucocorticoid-mediated inhibition of chemotherapy in ovarian carcinomas. Int J Oncol 28, 551-558.
Zhang, J.H., Chung, T.D.Y., and Oldenburg, K.R. (1999). A simple statistical parameter for use in evaluation and validation of high throughput screening assays. Journal of Biomolecular Screening 4, 67-73.
Zhang, X.M., Ramalho-Santos, M., and McMahon, A.P. (2001). Smoothened mutants reveal redundant roles for Shh and Ihh signaling including regulation of L/R symmetry by the mouse node. Cell 106, 781-792.

Figure Legends:

Fig.1. Glucocorticoids induce Smo accumulation at the primary cilium. **(A)** Structures of 10 representative naturally occurring and synthetic GCs (names in **bold**). **(B)** Related dose response

curves for accumulation of Smo in the PC using the subset of GCs indicated in (A). The mean (±S.D.) was calculated for four replicates analyzing several hundred cells in each sample. **(C)** Key positions correlating with Smo accumulation activity in the GC scaffold are highlighted in red. **(D)** Representative images of dose-dependent accumulation of Smo at the PC in response to stimulation by a synthetic GC, fluocinolone acetonide (FA). Scale bar: 10 μm.

Fig.2. FA sensitizes cells to Hh stimulation and competes with Cyc binding to Smo **(A)** Modest but significant activation of the Hh pathway at high doses of FA, measured by a Gli responsive luciferase reporter activity in NIH/3T3 cells. FA action is blocked by Smo antagonists SANT-1 and Cyc. * $P < 0.0001$ (t-test), comparing with DMSO, FA+SANT-1, or FA+Cyc. **(B)** FA up-regulates the expression of Hh target genes *Ptch1* and *Gli1* in NIH/3T3 cells. #$P<0.02$ (t-test) **(C-D)** Measurement of Hh pathway activity in cells treated simultaneously with a fixed concentration of FA and different concentrations of Shh ligand (C), or with a fixed concentration of Shh ligand, and different concentrations of FA (D). Treatment with Shh ligand and DMSO were used for comparison. **(E)** Measurement of Hh pathway activity after stimulation with various concentrations of Shh ligand following priming treatments with 10 μM FA (red curve). DMSO prime treatments (blue curve) were used for comparison. **(F)** Measurement of Hh pathway activity after stimulation with a fixed dose of Shh ligand following priming treatments with different concentrations of FA (red curve) or when pathway activity was stimulated by expressing a constitutively active SmoM2 variant (blue curve). All Gli-luciferase assay samples were replicated four times. The qRT-PCR in (B) was performed in triplicate. Data represent mean (±S.D.). **(G)** Schematics showing the structures of Bodipy-Cyc and Smo. Critical sites in the 6th and 7th transmembrane domains of Smo, that are likely important for direct interactions

are highlighted by rectangles. **(H)** Representative merged images from Bodipy-Cyc competition assays. Transfected cells can be identified by co-labeling with nuclear localized tagRFPT. **(I)** Quantification of Bodipy-Cyc fluorescence signal: each data point represents values from 50-100 transfected cells. The controls, including data from a parental plasmid(pCIT), Smo and SmoM2 expressing cells were displayed as the dashed lines. Mean (±S.D.) was calculated from four replicate samples. Scale bar: 10 μm.

Fig. 3. Drug-drug interaction between FA and GDC0449. **(A)** GDC0449 dose-dependent inhibition of Shh stimulated Hh pathway activity in the presence or absence of 10 μM FA, or SmoM2 expressing cell lines. **(B)** Representative images of Smo::EGFP/Ivs::tagRFPT cells treated with GDC0449 and Shh in the presence or absence of 10 μM FA. GDC0449 was co-applied at 111nM and 1,111nM respectively with Shh and Shh+FA. **(C)** Relative Smo::EGFP+ cilium count of GDC0449's dose-dependent inhibition of Shh-ligand stimulated accumulation of ciliary Smo in the presence or absence of 10 μM FA. Measurements were performed in quadruplicate. Several hundred cells were analyzed in each sample to assess the accumulation of Smo in the PC from data in (B). Data plotted are mean (±S.D.). Scale bar: 5 μm.

Fig.4. FA modulates proliferation of cerebellar granule-cell neural progenitors (CGNP). CGNP proliferation was quantified based on percentage of pH3 positive cells. Representative images and measurements were shown for FA dose dependent modulation of CGNP proliferation (A-B), promotion of Shh stimulated NP proliferation by 10 μM FA(C-D), and GDC0449 dose-dependent inhibition of Shh stimulated CGNP proliferation in the presence or absence of 10 μM FA(E-F). GDC0449 was applied at 100nM in (E). Mean (±S.D.) was calculated from four

replicate samples each containing over a thousand cells. *p=0.0003(t-test). #p<0.0001(t-test). Scale bar: 20 µm.

Fig.5. Bud inhibits Hh pathway activity induced by various stimuli and does not compete with Cyc for binding Smo. **(A)** The chemical structure of Bud. **(B-C)** representative images (B) and quantification of Smo ciliary localization (C) in Smo::EGFP/Ivs::tagRFPT cells treated with Shh and varying concentrations of Bud. **(D)** Measurement of Hh pathway activity in cells treated with Bud only or Bud followed by Shh. **(E)** Dose dependent inhibition of Hh pathway activity by Bud on Shh or SAG treatment, 50nM or 1 µM, respectively. **(F-G)** representative images (F) and quantification of Smo::EGFP or SmoM2::EGFP ciliary intensity (G) from cells treated with Bud. Bud was used at 22.2 µM in (F). **(H)** Bud's dose dependent inhibition of Hh pathway activity induced by overexpression of wildtype Smo and SmoM2 respectively. **(I)** Bud's dose dependent inhibition of Hh pathway activity induced by Shh ligand in Smo-/- cells transfected with constructs expressing wildtype Smo and SmoD473H respectively. **(J-K)** representative images (J) and quantification of Smo::EGFP or SmoD473H::EGFP ciliary intensity (K) from cells treated with Bud. **(L)** Measurement of Hh pathway activity in suFU-/- cells treated with Bud and FA respectively. DMSO and SAG were used as negative control and GANT61 was positive control. **(M-N)** representative images (M) and quantification of Bodipy-Cyc intensity in Smo expressing cos7 cells (N) treated with Bodipy-Cyc and Bud. Vehicle was used for comparison. Bud was used at 200 µM in (M). All quantitative data represent mean (±S.D.) from either quadruplicated samples (imaging assays) or triplicate experiments (Gli-luciferase assays). Quantifications of ciliary localization involved over a thousand cells per sample whereas 50-100

Smo expressing cells were analyzed in each treatment for Bodipy-Cyc competition assay. Scale bar: 5 μm.

Fig. 6. GDC0449 and Bud combinatorially inhibit Smo-directed Hedgehog signaling. **(A-B)** Quantification of Smo ciliary localization (A) and representative images (B) of Smo::EGFP/Ivs::tagRFPT cells treated with GDC0449 and Shh in the presence or absence of 10 μM Bud. In (A), GDC0449 was co-applied at 1.6nM with Shh and Shh+Bud respectively. **(C)** GDC0449 dose-dependent inhibition of Shh stimulated Hh pathway activity in the presence or absence of 10 μM Bud. Data plotted are mean (±S.D.) from four biological replicates (B) analyzing over a thousand of cells or three biological replicates(C). Scale bar: 5 μm.

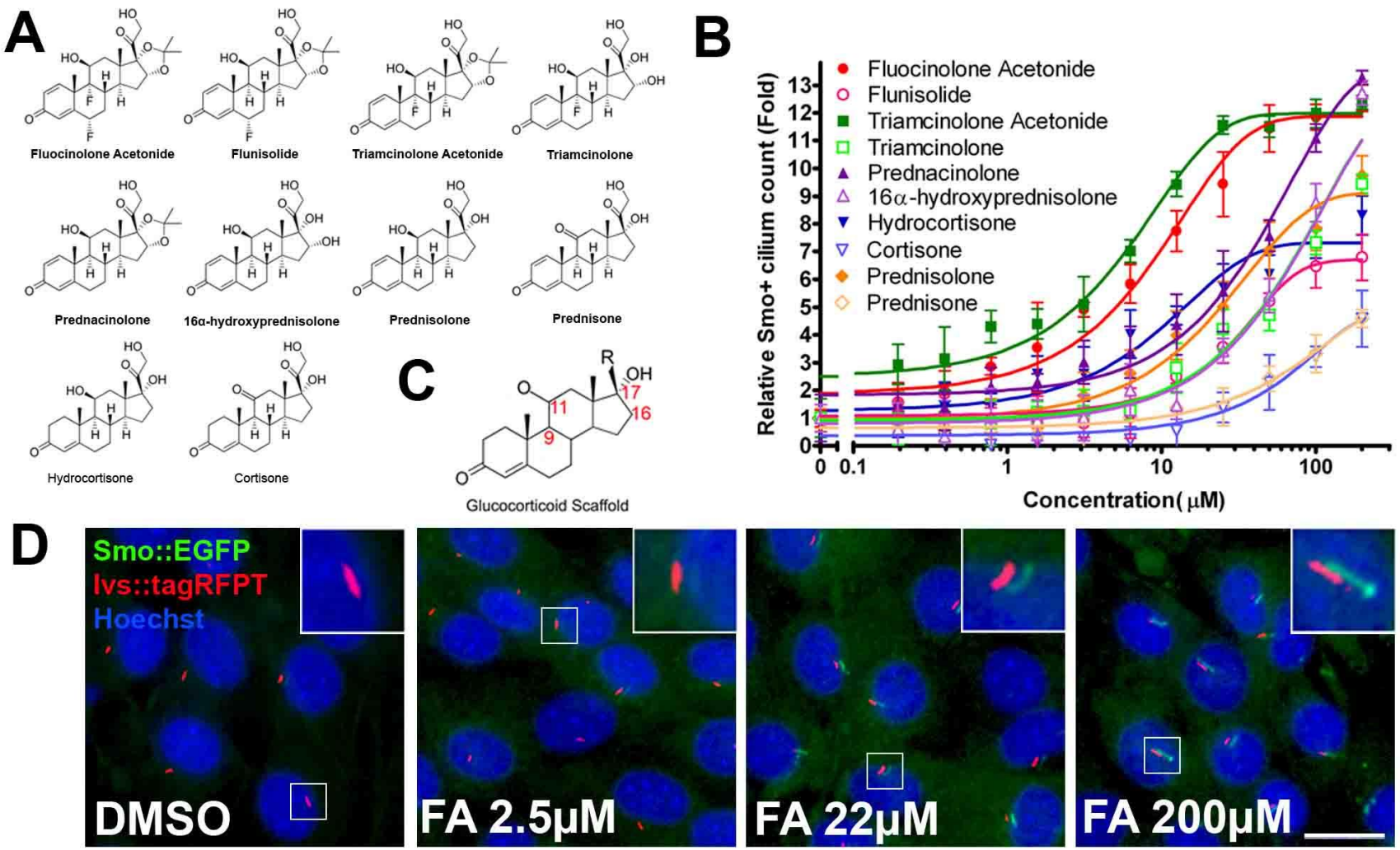
A
Fluocinolone Acetonide
Flunisolide
Triamcinolone Acetonide
Triamcinolone
Prednacinolone
16α-hydroxyprednisolone
Prednisolone
Prednisone
Hydrocortisone
Cortisone
C
Glucocorticoid Scaffold
B
Fluocinolone Acetonide
Flunisolide
Triamcinolone Acetonide
Triamcinolone
Prednacinolone
16α-hydroxyprednisolone
Hydrocortisone
Cortisone
Prednisolone
Prednisone
Relative Smo+ cilium count (Fold)
Concentration(μM)
D
Smo::EGFP
Ivs::tagRFPT
Hoechst
DMSO
FA 2.5μM
FA 22μM
FA 200μM

Fig. 1

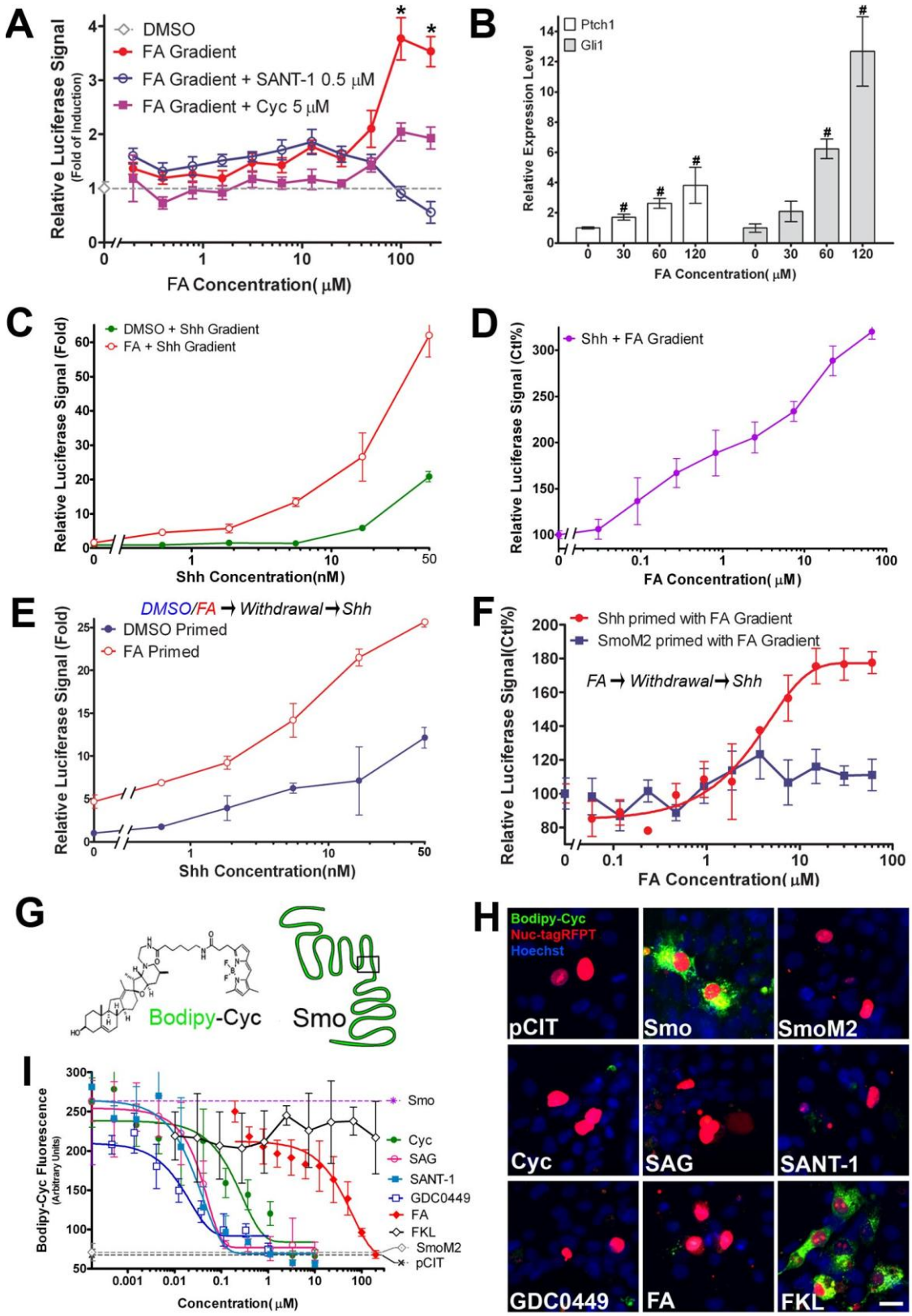
A
DMSO
FA Gradient
FA Gradient + SANT-1 0.5 μM
FA Gradient + Cyc 5 μM
Relative Luciferase Signal
(Fold of Induction)
FA Concentration(μM)
B
Ptch1
Gli1
Relative Expression Level
FA Concentration(μM)
C
DMSO + Shh Gradient
FA + Shh Gradient
Relative Luciferase Signal (Fold)
Shh Concentration(nM)
D
Shh + FA Gradient
Relative Luciferase Signal (Ctl%)
FA Concentration(μM)
E
DMSO/FA → Withdrawal → Shh
DMSO Primed
FA Primed
Relative Luciferase Signal (Fold)
Shh Concentration(nM)
F
Shh primed with FA Gradient
SmoM2 primed with FA Gradient
FA → Withdrawal → Shh
Relative Luciferase Signal(Ctl%)
FA Concentration(μM)
G
Bodipy-Cyc
Smo
H
Bodipy-Cyc
Nuc-tagRFPT
Hoechst
pCIT
Smo
SmoM2
Cyc
SAG
SANT-1
GDC0449
FA
FKL
I
Bodipy-Cyc Fluorescence
(Arbitrary Units)
Smo
Cyc
SAG
SANT-1
GDC0449
FA
FKL
SmoM2
pCIT
Concentration(μM)

Fig.2

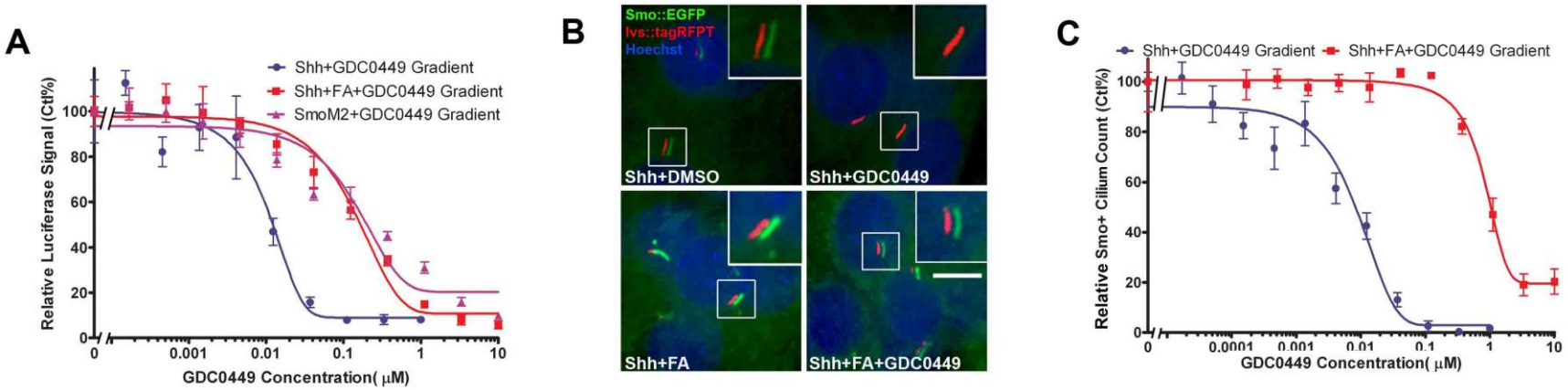
A
Shh+GDC0449 Gradient
Shh+FA+GDC0449 Gradient
SmoM2+GDC0449 Gradient
Relative Luciferase Signal (Ctl%)
GDC0449 Concentration(μM)
B
Smo::EGFP
Ivs::tagRFPT
Hoechst
Shh+DMSO
Shh+GDC0449
Shh+FA
Shh+FA+GDC0449
C
Shh+GDC0449 Gradient
Shh+FA+GDC0449 Gradient
Relative Smo+ Cilium Count (Ctl%)
GDC0449 Concentration(μM)

Fig.3

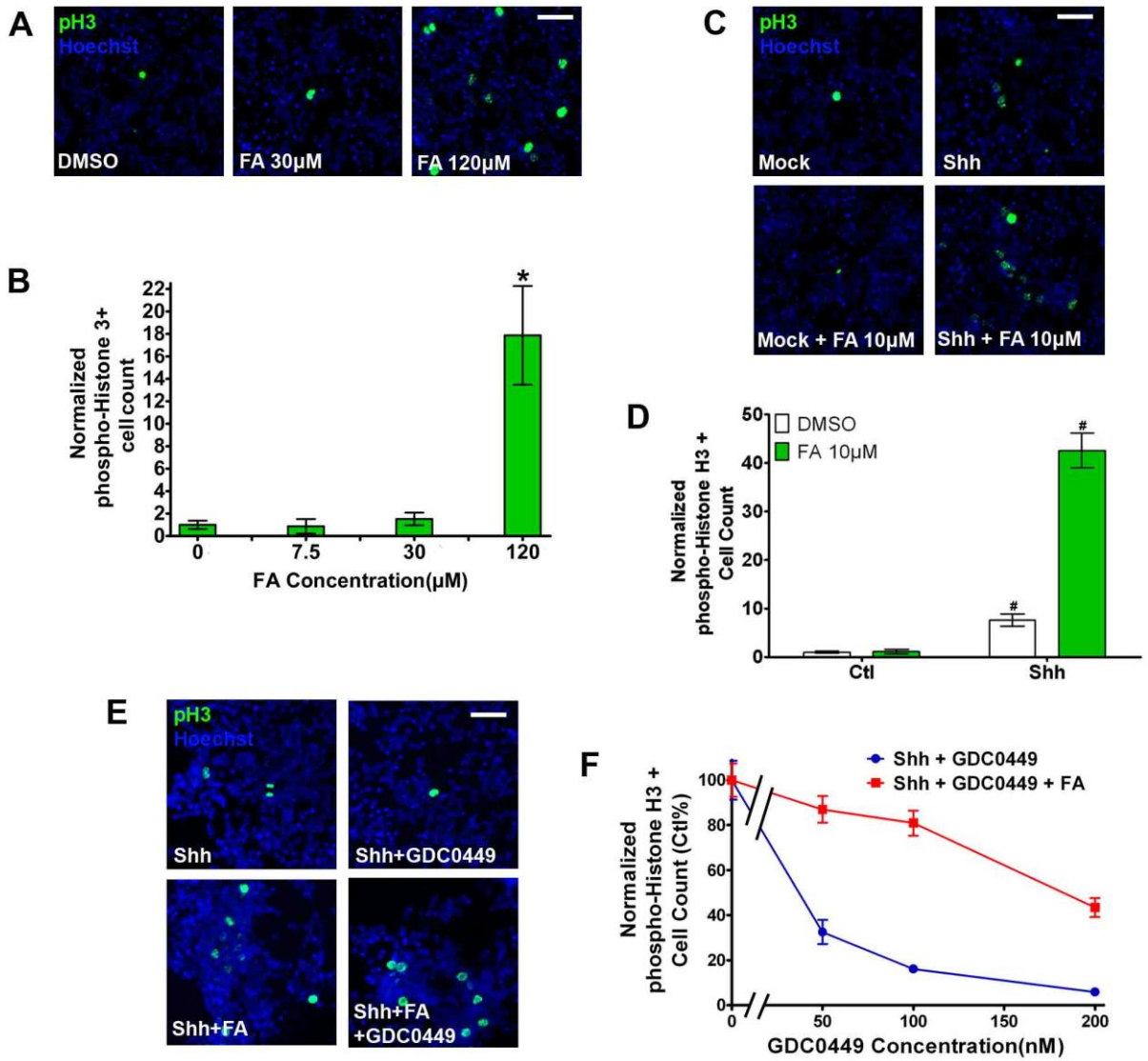
A
pH3
Hoechst
DMSO
FA 30μM
FA 120μM
B
Normalized phospho-Histone 3+ cell count
FA Concentration(μM)
0
7.5
30
120
C
pH3
Hoechst
Mock
Shh
Mock + FA 10μM
Shh + FA 10μM
D
DMSO
FA 10μM
Normalized phospho-Histone H3 + Cell Count
Ctl
Shh
E
pH3
Hoechst
Shh
Shh+GDC0449
Shh+FA
Shh+FA +GDC0449
F
Shh + GDC0449
Shh + GDC0449 + FA
Normalized phospho-Histone H3 + Cell Count (Ctl%)
GDC0449 Concentration(nM)

Fig. 4

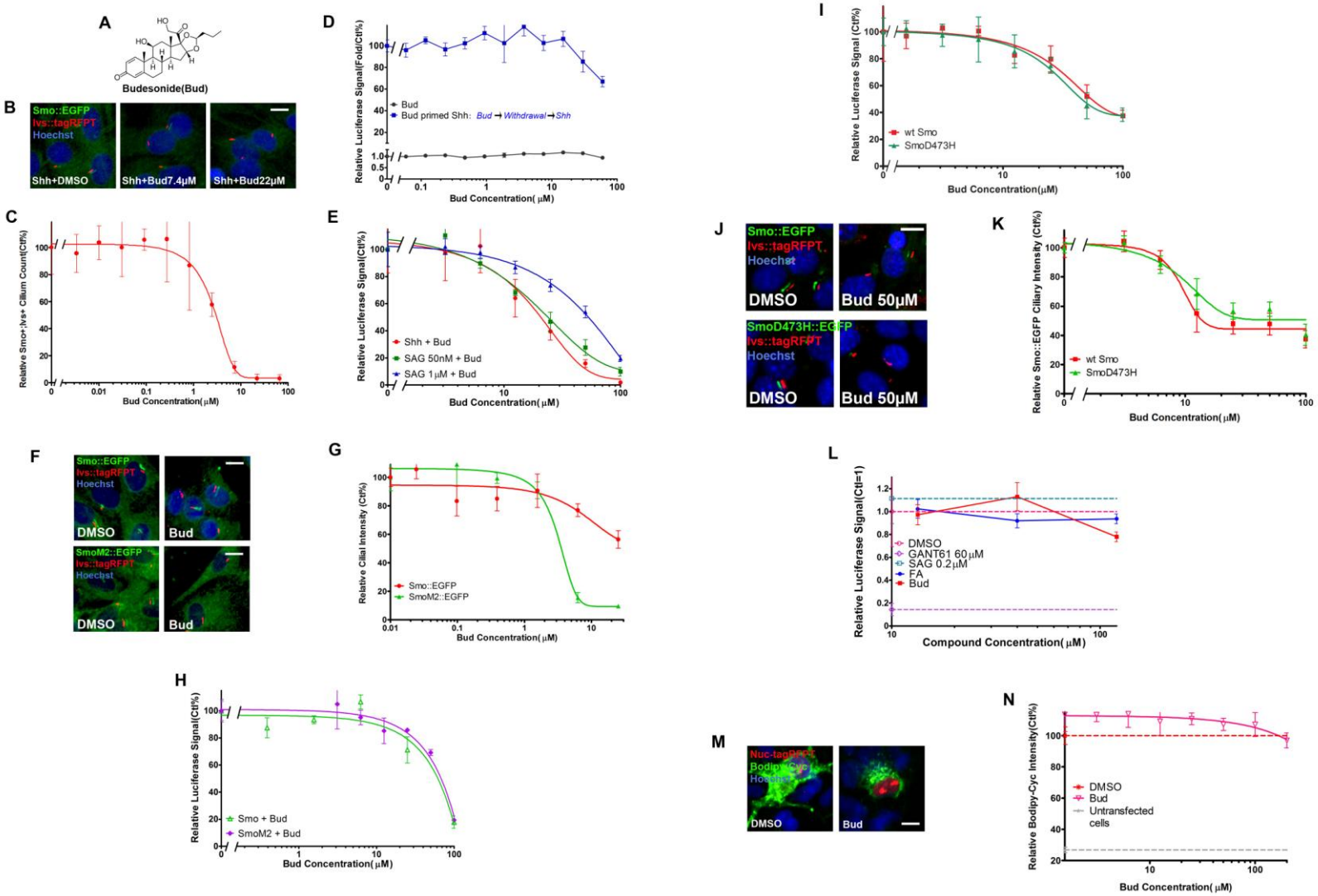
A
Budesonide(Bud)
B
Smo::EGFP
Ivs::tagRFPT
Hoechst
Shh+DMSO
Shh+Bud7.4μM
Shh+Bud22μM
C
Relative Smo+:Ivs+ Cilium Count(Ctl%)
Bud Concentration(μM)
D
Relative Luciferase Signal(Fold/Ctl%)
Bud
Bud primed Shh: Bud → Withdrawal → Shh
Bud Concentration(μM)
E
Relative Luciferase Signal(Ctl%)
Shh + Bud
SAG 50nM + Bud
SAG 1μM + Bud
Bud Concentration(μM)
F
Smo::EGFP
Ivs::tagRFPT
Hoechst
DMSO
Bud
SmoM2::EGFP
Ivs::tagRFPT
Hoechst
DMSO
Bud
G
Relative Cilial Intensity (Ctl%)
Smo::EGFP
SmoM2::EGFP
Bud Concentration(μM)
H
Relative Luciferase Signal(Ctl%)
Smo + Bud
SmoM2 + Bud
Bud Concentration(μM)
I
Relative Luciferase Signal (Ctl%)
wt Smo
SmoD473H
Bud Concentration(μM)
J
Smo::EGFP
Ivs::tagRFPT
Hoechst
DMSO
Bud 50μM
SmoD473H::EGFP
Ivs::tagRFPT
Hoechst
DMSO
Bud 50μM
K
Relative Smo::EGFP Ciliary Intensity (Ctl%)
wt Smo
SmoD473H
Bud Concentration(μM)
L
Relative Luciferase Signal(Ctl=1)
DMSO
GANT61 60μM
SAG 0.2μM
FA
Bud
Compound Concentration(μM)
M
Nuc-tagRFPT
Bodipy-Cyc
Hoechst
DMSO
Bud
N
Relative Bodipy-Cyc Intensity(Ctl%)
DMSO
Bud
Untransfected cells
Bud Concentration(μM)

Fig. 5

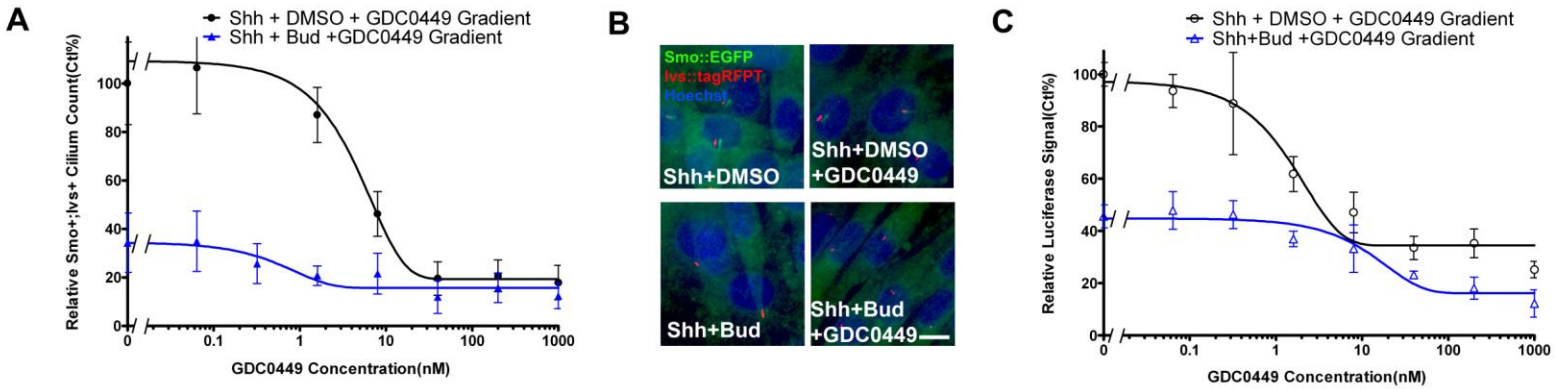
A
Shh + DMSO + GDC0449 Gradient
Shh + Bud +GDC0449 Gradient
Relative Smo+;Ivs+ Cilium Count(Ctl%)
GDC0449 Concentration(nM)
B
Smo::EGFP
Ivs::tagRFPT
Hoechst
Shh+DMSO
Shh+DMSO +GDC0449
Shh+Bud
Shh+Bud +GDC0449
C
Shh + DMSO + GDC0449 Gradient
Shh+Bud +GDC0449 Gradient
Relative Luciferase Signal(Ctl%)
GDC0449 Concentration(nM)

Fig. 6

Glucocorticoid Compounds Modify Smoothened Localization and Hedgehog Pathway Activity

Yu Wang *et al.*

Supplementary Figures (S1-S5)

Supplementary Figure Legends:

Fig. S1(Related to Fig.1). A high content screen for compounds driving Smo ciliary tranlocation. **(A)** A 500nM solution of the small molecule Smo agonist SAG was serially diluted in low serum medium Smo::EGFP/Ivs::tagRFPT cells were treated with varying concentrations of SAG. Here and elsewhere, the Ivs::tagRFPT images were shifted leftwards by 5 pixels to show both Smo and Ivs signals in merged images. Scale bar: 5 µm. **(B)** Multi-parametric quantification of data sets in the high content assay: mean (±S.D.) from duplicate experiments are presented. **(C)**A 15 µM Cyc solution was serially diluted in low serum medium and introduced to Smo::EGFP/Ivs::tagRFPT cells. Scale bar: 10 µm. **(D)** Multi-parametric quantifications of data: mean from duplicate experiments. **(E)** A 200 µM solution of FKL was serially diluted in low serum medium and applied to Smo::EGFP/Ivs::tagRFPT cells. Note the lengthened cilium of treatment with FKL evident by lengthened Ivs::tagRFPT domain. Scale bar: 10 µm. **(F)** Multi-parametric quantification of data sets: mean (±S.D) from four replicates. **(G)** A Plot of relative Smo::EGFP+ cilium count normalized to cell number for putative agonist screen. Each dot represents the measurement of over a thousand cells in each well. Compound libraries were assayed at 10 µM. SANT-1 and SAG were used at 1 µM and Cyc at 10 µM. **(H)** The chemical structure of LY294002. **(I)** Representative images of Smo::EGFP/Ivs::tagRFPT cells treated with 30 µM LY294002 in comparison with DMSO vehicle only. Scale bar: 10 µm. **(J)** Quantification of Smo::EGFP positive cilia upon treatment with varying concentrations of LY294002 (red) and dose dependent inhibition of Shh ligand driven pathway activity by LY294002 (blue). **(K)** High content quantification of various parameters of treatment with varying concentrations of LY294002. Means (±S.D) from four replicates were presented. **(L)** Structures of all

glucocorticoids (in alphabetical order) demonstrated to promote Smo ciliary accumulation. **(M)** High content image analyses of Smo::EGFP/Ivs::tagRFPT cells treated with a different concentrations of FA. Measurements were performed in quadruplicate scoring several hundred cells in each sample. Data display mean values (±S.D). **(N)** Representative images of immunofluorescence of cilium markers including acetylated tubulin(acet-tub), detyrosinated α-tubulin(glu-tub), and Arl13b, and quantification of Arl13b measurements upon treatment with FA or the vehicle. **(O)** Wnt signaling activity as measured by Top-flash signal was not affected when FA was applied alone, simultaneously with Wnt3a ligand or whenreporter cells were pre-treated with FA prior to Wnt3a ligand addition. Measurements were performed in quadruplicate. Data display the mean (±S.D.).

Fig. S2(Related to Fig.2). Analyses of Smo ciliary accumulation induced by overexpression or FA. (**A)** Comparison of the dose-response required for activating the Hh pathway when over-expressing Smo (red curve) or GFP (green curve) in reporter cells. Experiments were performed in quadruplicate. Data display the mean (±S.D.). **(Inset)** A representative image of a Smo over-expressing cell line shows Smo accumulation in the PC in the absence of ligand. Scale bar: 10 μm. **(B)** Representative images taken immediately, 8hours, and 24 hours after FA(10 μM) withdrawal. **(C)** Time lapse plots of the fluorescent intensity of Smo::EGFP and Ivs::tagRFPT at the PC following FA(10 μM) withdrawal. Data display the mean (±S.D.) calculated from four repeats measuring several hundred cells in each sample. Scale bar: 5 μm.
(D) Measurements of Gli-luciferase activity of wildtype and Smo-/- MEF cells treated with FA and TA respectively. Data represent mean (±S.D.) of triplicated samples. P values from student t tests comparing with DMSO treated controls were labeled. “n.s.” stands for “non-significance”.

(E) Graphs of dose dependent reduction of FA driven Smo accumulation within the PC on increasing levels of SANT-1 and GDC0449. Mean (±S.D.) of relative number of Smo+ PC calculated from analysis of several hundred cells in quadruplicate treatments. **(F)** Representative images. Scale bar: 5 μm.

Fig. S3(Related to Fig.3). FA confers resistance to Hh pathway inhibition by the Smo antagonists Cyc and SANT-1. (**A-B)** Cyc (A) or SANT-1(B) mediated dose dependent inhibition of Shh ligand induced Hh pathway activation in the presence or absence of 10 μM FA. **(C)** SANT-1 mediated dose-dependent inhibition of Smo accumulation at the PC in response to Shh ligand stimulation in the presence or absence of 10 μM FA. **(D)** Representative images quantified in (C). SANT-1 was applied at 370nM. Measurements represent several hundred cells in quadruplicate samples. Data plotted display the mean (±S.D.). Scale bar: 5 μm.

Fig. S4(Related to Fig.1-3). Characterization of TA. **(A)** Significant activation of the Hh pathway only at high doses of TA, measured by a Gli responsive luciferase reporter activity in NIH/3T3 cells. * P=0.005 and **P < 0.0001 (t-test), comparing with DMSO. **(B)** Measurement of Hh pathway activity in cells treated simultaneously with a fixed concentration of TA (10μM) and different concentrations of Shh ligand Treatment with Shh ligand and DMSO were used for comparison. **(C-D)** Representative images(C) and quantification of Bodipy-Cyc fluorescence signal(D) from competition assays. The controls, including data from a parental plasmid(pCIT) and competition by SAG or Cyc, were displayed. Mean (±S.D.) was calculated from four replicate samples. Scale bar: 10μm. **(E)** GDC0449 dose-dependent inhibition of Shh stimulated Hh pathway activity in the presence or absence of 10 μM TA. **(F)** Representative images of

Smo::EGFP/Ivs::tagRFPT cells treated with GDC0449 and Shh in the presence or absence of 10 μM TA. GDC0449 was co-applied at 15.6nM with Shh+DMSO or Shh+TA. **(G)** Relative Smo::EGFP ciliary intensity of GDC0449's dose-dependent inhibition of Shh induced Smo ciliary accumulation in the presence or absence of 10 μM TA. Measurements were performed in quadruplicate. Several hundred cells were analyzed in each sample to assess the accumulation of Smo in the PC. Data plotted are mean (±S.D.). Scale bar: 5 μm. All Gli-luciferase assay samples corresponding to this figure were replicated three times.

Fig. S5(Related to Fig.5). Analyses of GC Smo antagonists, Cic and Bud. (**A)** Cic structure. **(B)** representative images of Shh treated Smo::EGFP/Ivs::tagRFPT cells with DMSO or Cic at 30 μM. Scale bar: 5 μm. **(C)** Quantification of Smo ciliary localization of cells treated with Shh and various doses of Cic. Measurements represent several hundred cells in quadruplicate samples. Data plotted display the mean (±S.D.). **(D)** Cic dose-dependent inhibition of Hh pathway activity measured by a Gli responsive luciferase reporter activity in NIH/3T3 cells. Data plotted display the mean (±S.D.) of triplicate samples. **(E)** Representative images of Smo::EGFP/Ivs::tagRFPT cells treated with 100 μM Bud and 5 μM Cyc or varying doses of SAG. DMSO was a vehicle control for comparison. Scale bar: 5 μm. **(F)** Quantification of Bud's dose-dependent inhibition of Smo::EGFP ciliary intensity induced by SAG or Cyc. Measurements represent several hundred cells in quadruplicate samples. Data plotted display the mean (±S.D.). **(G)** Wnt signaling activity in a Top-flash reporter assay was not affected when Bud was applied alone, simultaneously with Wnt3a ligand or by pre-treating reporter cells prior to Wnt3a ligand addition. Measurements were performed in quadruplicate. Data display the mean (±S.D.). **(H and J)** Representative images of Smo::EGFP and SmoM2::EGFP overexpressing cells treated with 370nM SANT-1 (H)

or 370nM GDC0449 (J). DMSO was used as a control for comparison. Scale bar: 5 µm. **(I and K)** Quantification of ciliary intensity of Smo::EGFP and SmoM2::EGFP for cells treated with varying concentrations of SANT-1(I) or GDC0449(K). Data plotted display the mean (±S.D.) from triplicate experiments. **(L)** Representative images of Smo::EGFP and SmoM2::EGFP overexpressing cells treated with 100 µM Cic. DMSO was used as a control for comparison. Both Ivs::tagRFPT and acetylated tubulin (acet-tub) were examined as markers enriched in the PC. Scale bar: 5 µm. **(M-O)** Quantification of Smo::EGFP and SmoM2::EGFP ciliary intensity (M), Ivs::tagRFPT ciliary intensity (N), and Ivs::tagRFPT positive cilium count (O). Measurements represent several hundred cells in quadruplicate samples. Data plotted display the mean (±S.D.). **(P)** High content quantification of Smo::EGFP/Ivs::tagRFPT cells treated with Shh and varying concentrations of Bud. Measurements represent several hundred cells in quadruplicate samples. Data plotted display the mean (±S.D.). **(Q)**Comparative analysis of Arl13b::tagRFPT and acet-tub in the PC of cells treated with 100 µM Bud or DMSO vehicle. Scale bar: 5 µm. **(R)** Quantitative analyses of Arl13b::tagRFPT positive primary cilia upon Bud treatment. Measurements represent several hundred cells in quadruplicate samples. Data plotted display the mean (±S.D.). **(S)** Measurements of Gli-luciferase activity in Smo-/- MEF cells tranfected with a plasmid expressing GFP, wildtype Smo, or SmoD473H, and treated with BSA or Shh. **(T)** Dose reponse measurements of GDC0449 for Shh induced Gli-luciferase activity in Smo-/- MEF cells expressing wildtype Smo or SmoD473H. **(U-V)** representative images(U) and dose response measurements of ciliary EGFP intensity that is fused to either wildtype Smo or SmoD473H and expressed in 3T3 cells, upon treatment with GDC0449.

Supplementary Figures

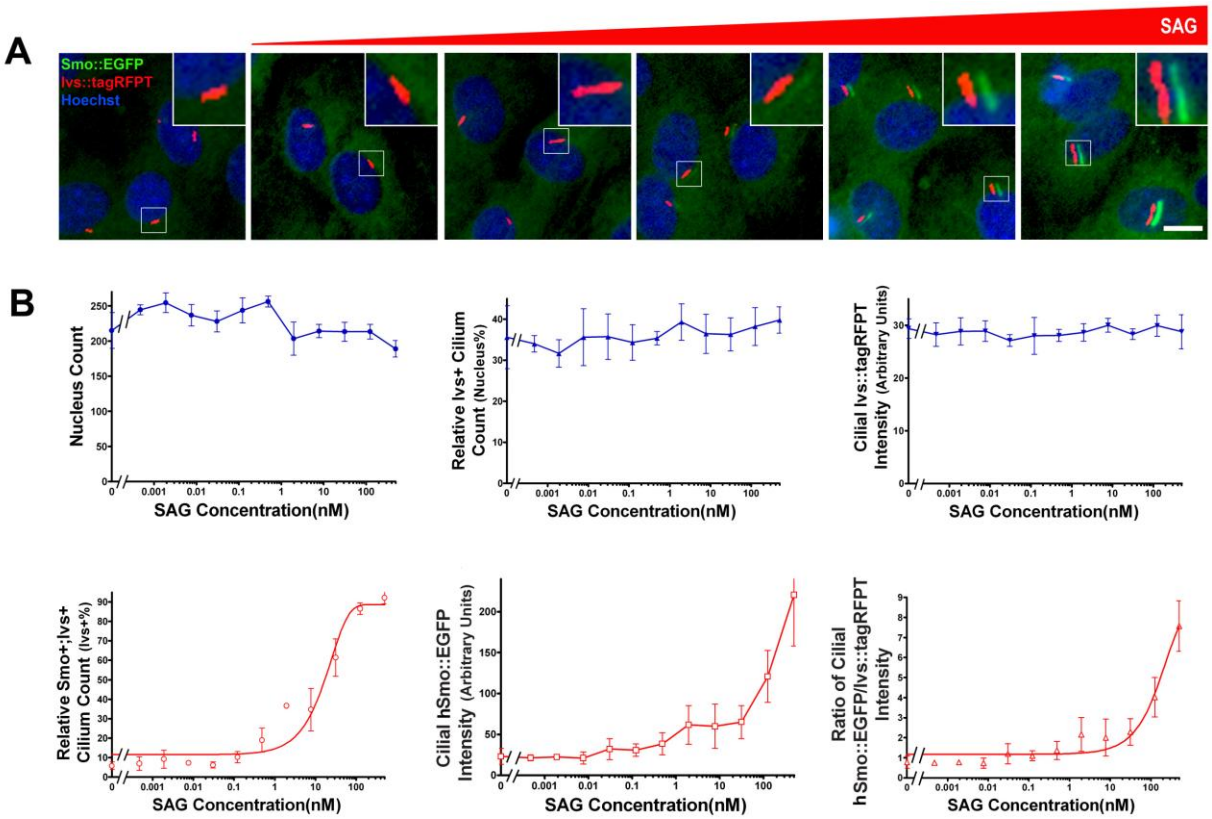

Fig.S1

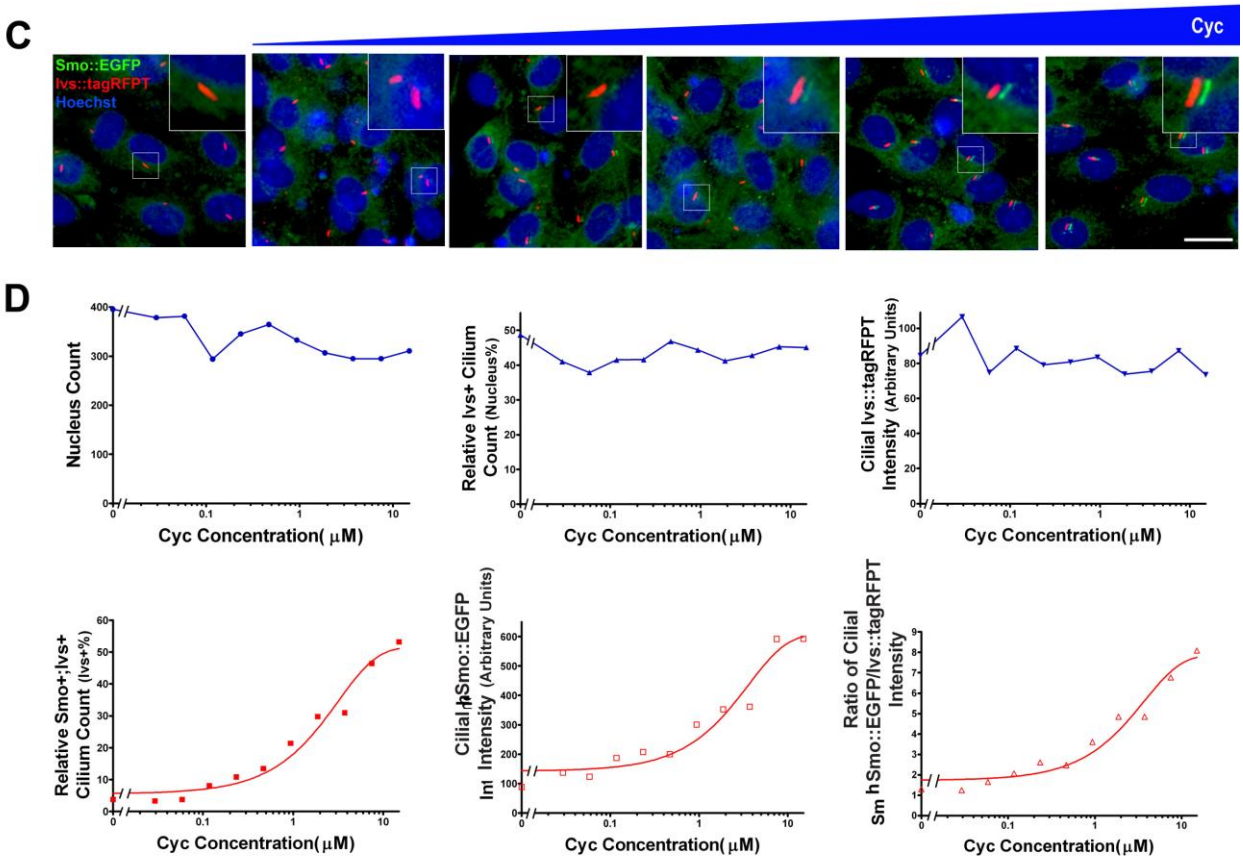

Fig. S1 (Continued)

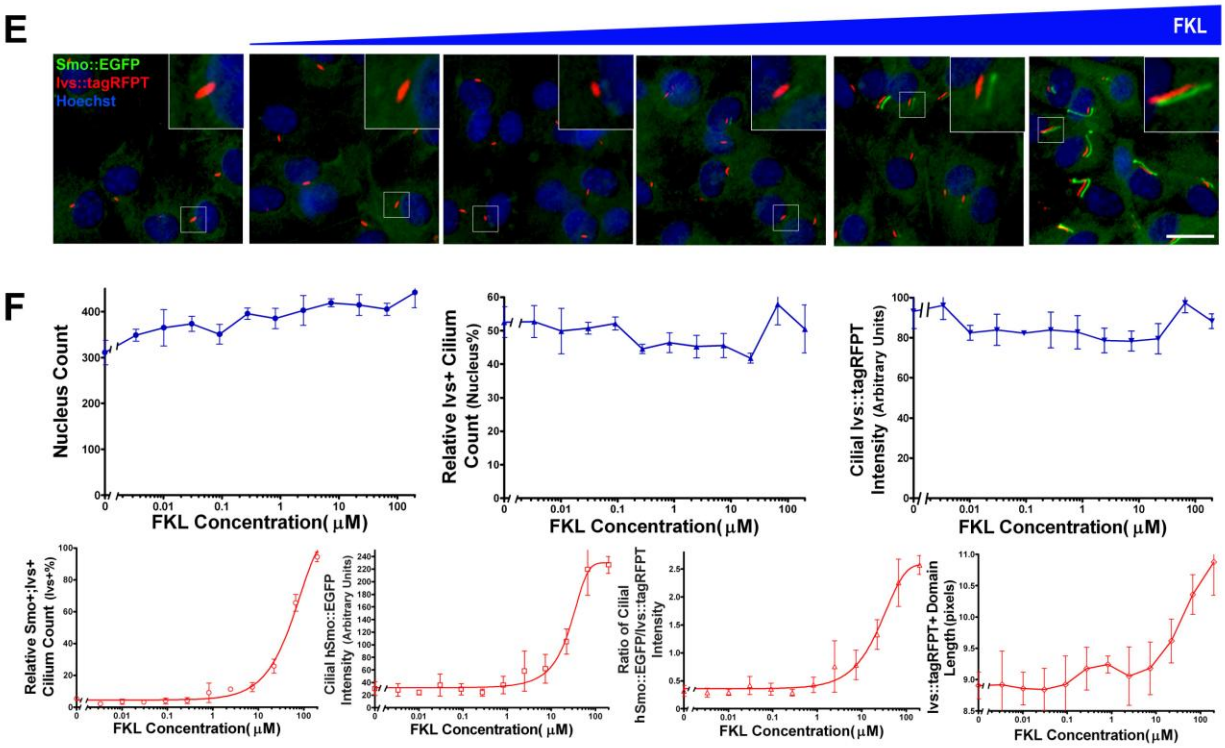

Fig. S1 (Continued)

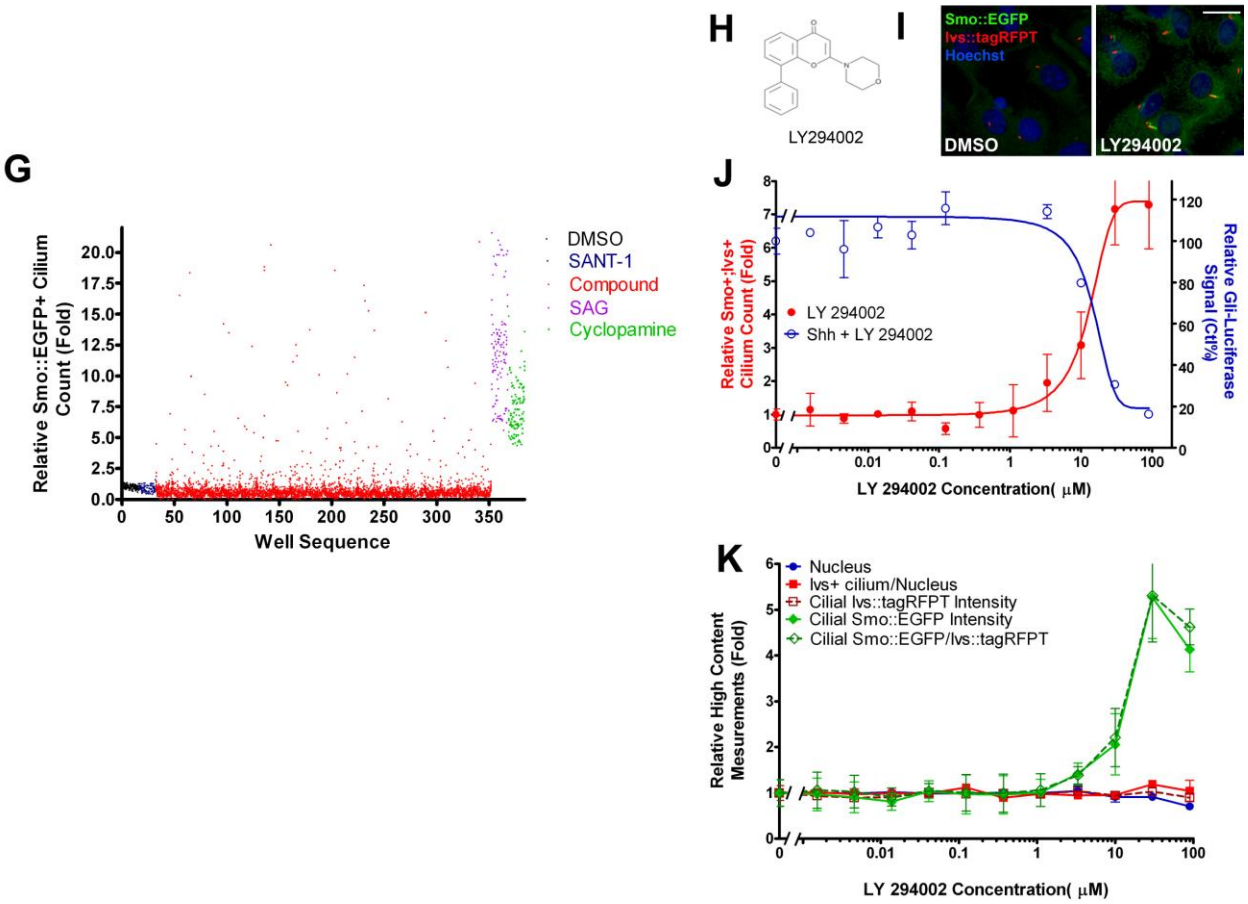

Fig. S1 (Continued)

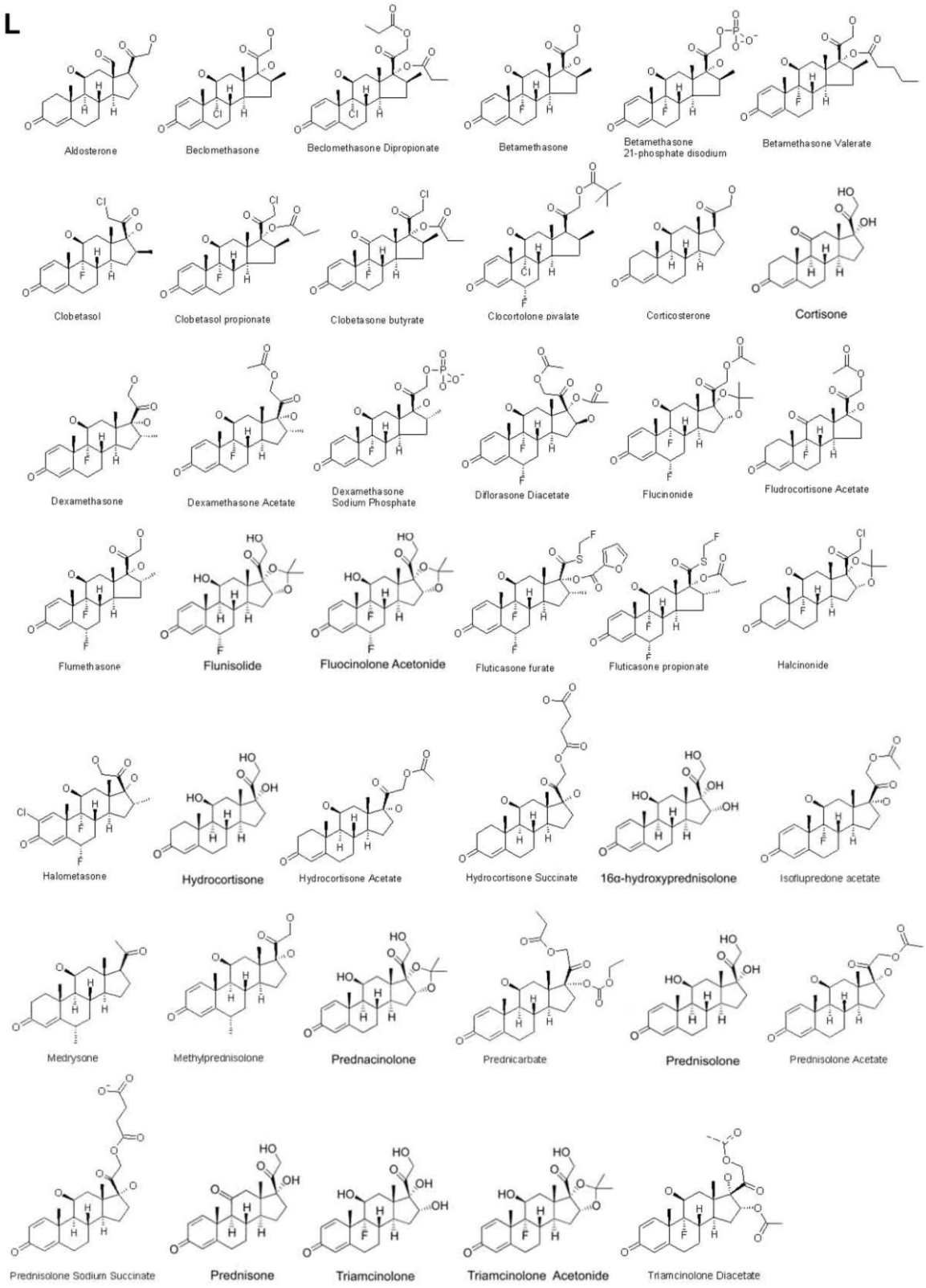

Fig. S1 (Continued)

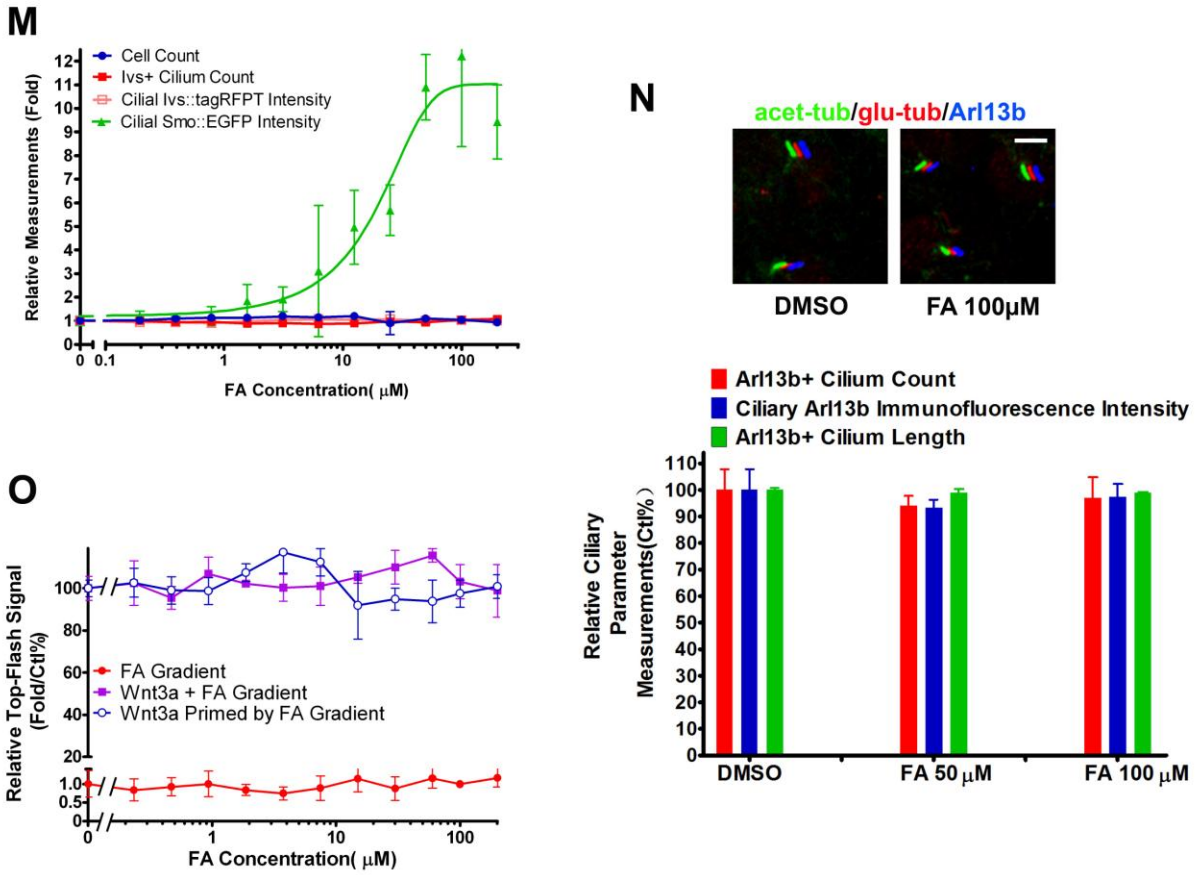

Fig. S1 (Continued)

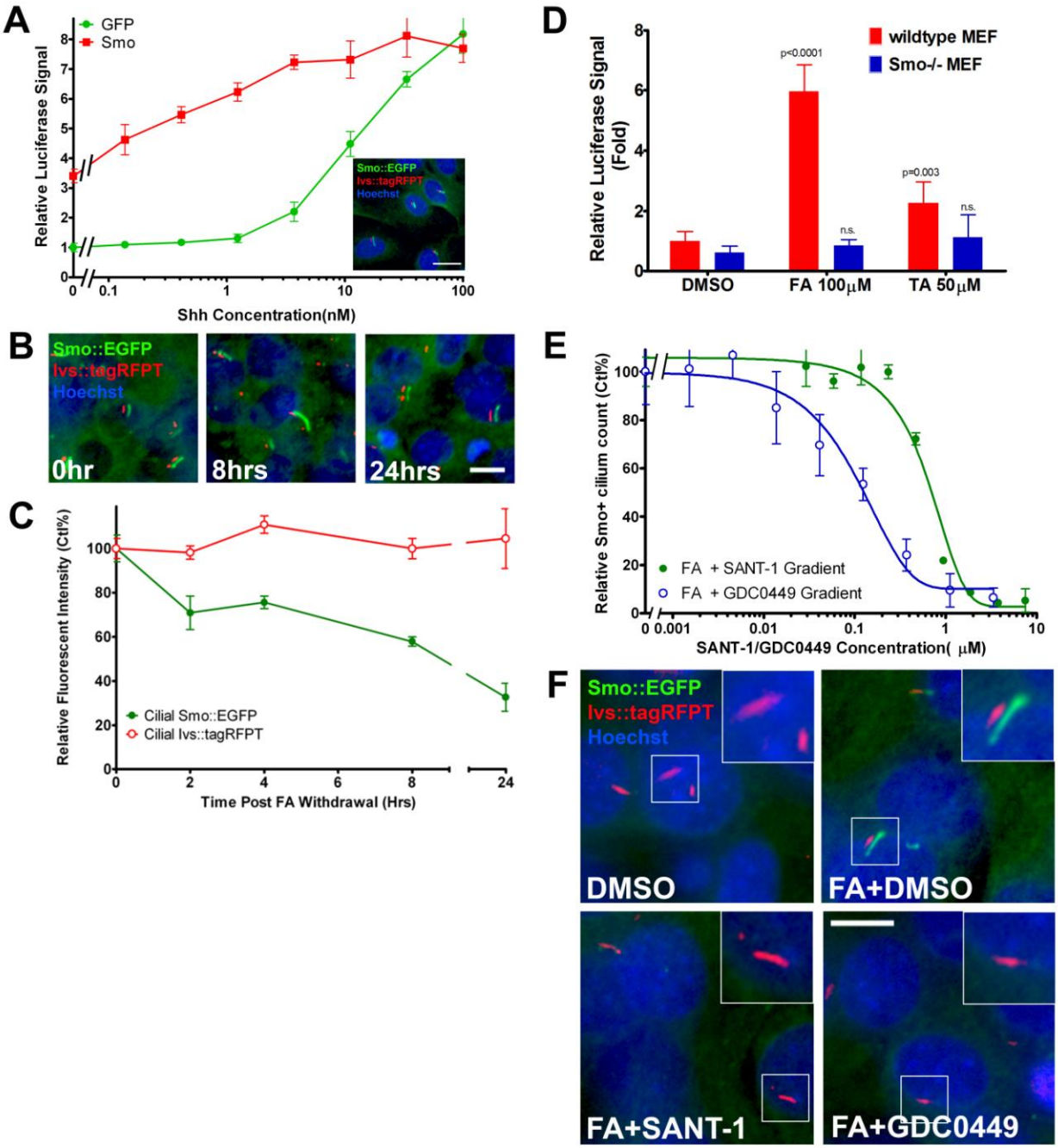
A
GFP
Smo
Relative Luciferase Signal
Shh Concentration(nM)
Smo::EGFP
Ivs::tagRFPT
Hoechst
B
Smo::EGFP
Ivs::tagRFPT
Hoechst
0hr
8hrs
24hrs
C
Relative Fluorescent Intensity (Ctl%)
Cilial Smo::EGFP
Cilial Ivs::tagRFPT
Time Post FA Withdrawal (Hrs)
D
wildtype MEF
Smo-/- MEF
Relative Luciferase Signal (Fold)
p<0.0001
p=0.003
n.s.
n.s.
DMSO
FA 100μM
TA 50μM
E
Relative Smo+ cilium count (Ctl%)
FA + SANT-1 Gradient
FA + GDC0449 Gradient
SANT-1/GDC0449 Concentration(μM)
F
Smo::EGFP
Ivs::tagRFPT
Hoechst
DMSO
FA+DMSO
FA+SANT-1
FA+GDC0449

Fig. S2

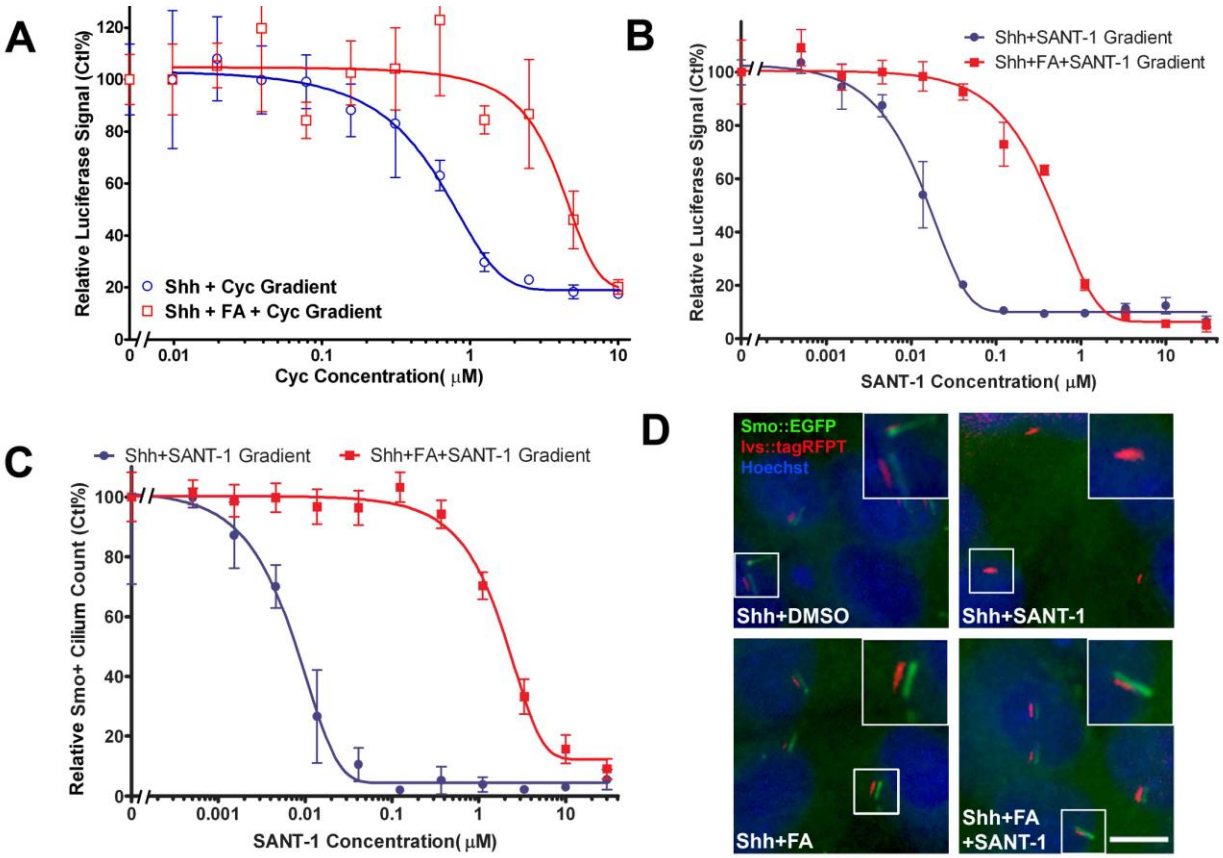
A
Relative Luciferase Signal (Ctl%)
Shh + Cyc Gradient
Shh + FA + Cyc Gradient
Cyc Concentration(μM)
B
Shh+SANT-1 Gradient
Shh+FA+SANT-1 Gradient
Relative Luciferase Signal (Ctl%)
SANT-1 Concentration(μM)
C
Shh+SANT-1 Gradient
Shh+FA+SANT-1 Gradient
Relative Smo+ Cilium Count (Ctl%)
SANT-1 Concentration(μM)
D
Smo::EGFP
Ivs::tagRFPT
Hoechst
Shh+DMSO
Shh+SANT-1
Shh+FA
Shh+FA
+SANT-1

Fig. S3

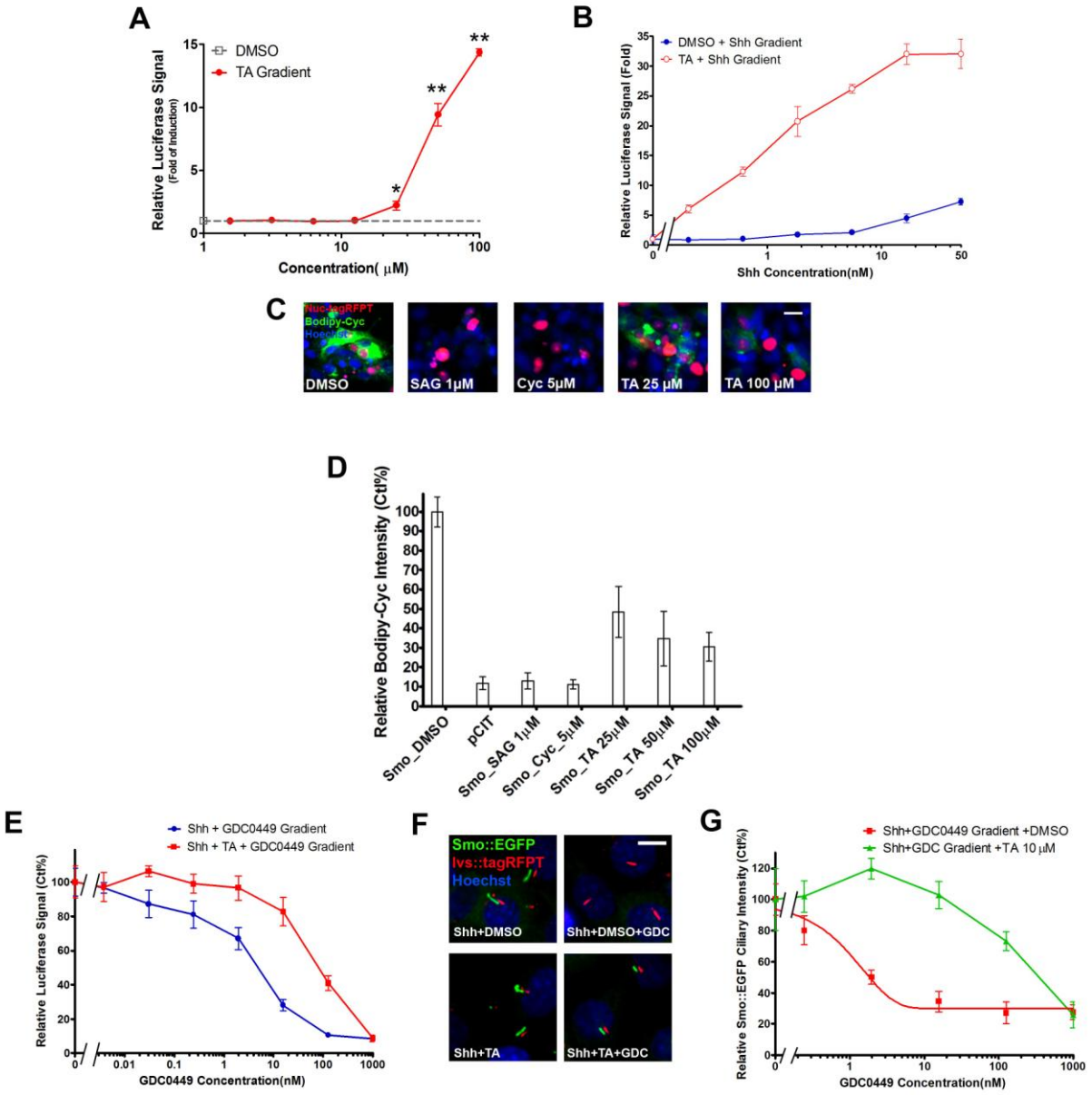
A
DMSO
TA Gradient
Relative Luciferase Signal
(Fold of Induction)
Concentration(μM)
B
DMSO + Shh Gradient
TA + Shh Gradient
Relative Luciferase Signal (Fold)
Shh Concentration(nM)
C
Nuc-tagRFPT
Bodipy-Cyc
Hoechst
DMSO
SAG 1μM
Cyc 5μM
TA 25 μM
TA 100 μM
D
Relative Bodipy-Cyc Intensity (Ctl%)
Smo_DMSO
pCIT
Smo_SAG 1μM
Smo_Cyc_5μM
Smo_TA 25μM
Smo_TA 50μM
Smo_TA 100μM
E
Shh + GDC0449 Gradient
Shh + TA + GDC0449 Gradient
Relative Luciferase Signal (Ctl%)
GDC0449 Concentration(nM)
F
Smo::EGFP
Ivs::tagRFPT
Hoechst
Shh+DMSO
Shh+DMSO+GDC
Shh+TA
Shh+TA+GDC
G
Shh+GDC0449 Gradient +DMSO
Shh+GDC Gradient +TA 10 μM
Relative Smo::EGFP Ciliary Intensity (Ctl%)
GDC0449 Concentration(nM)

Fig.S4

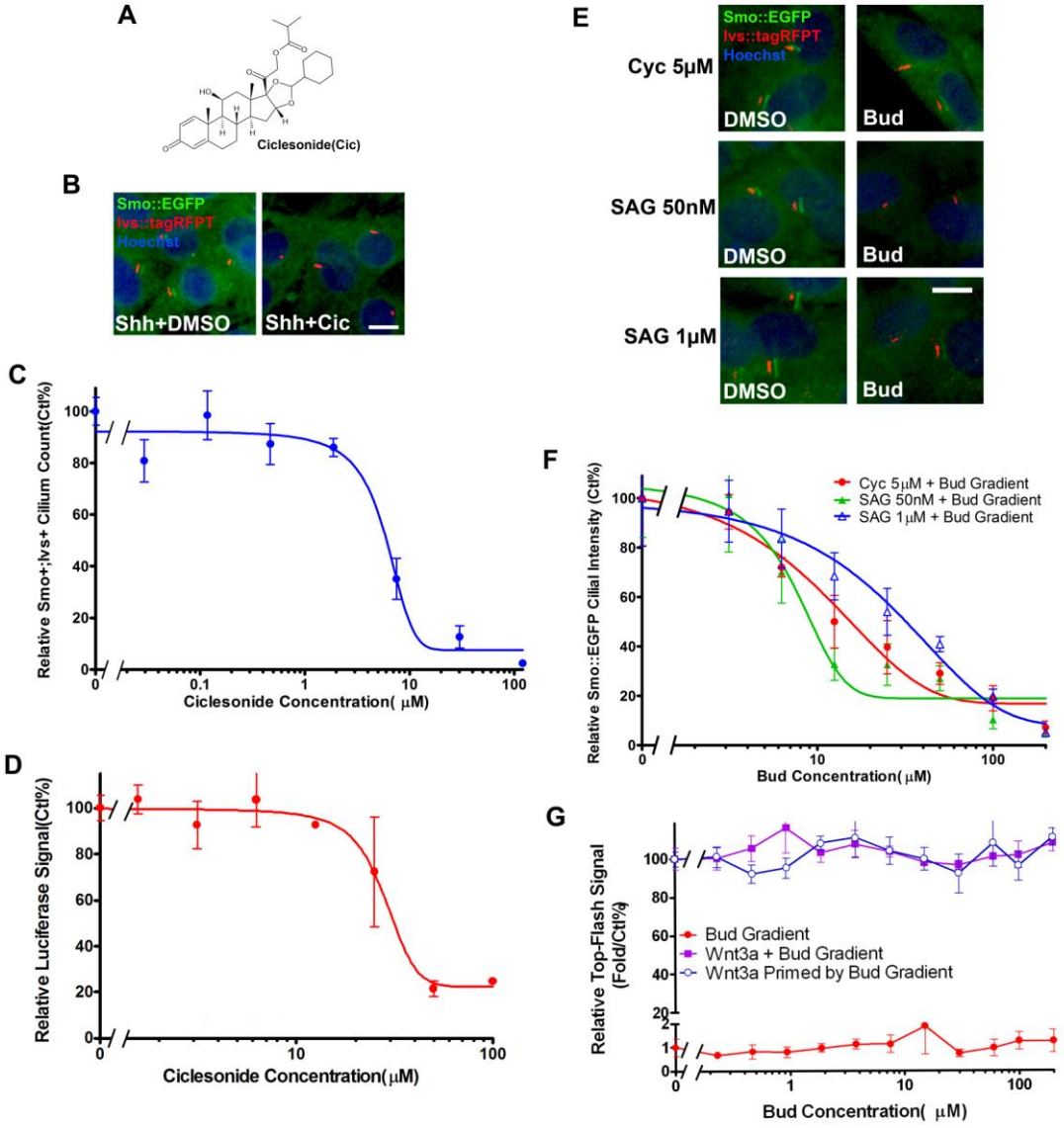
A
Ciclesonide(Cic)
B
Smo::EGFP
Ivs::tagRFPT
Hoechst
Shh+DMSO
Shh+Cic
C
Relative Smo+;Ivs+ Cilium Count(Ctl%)
Ciclesonide Concentration(μM)
D
Relative Luciferase Signal(Ctl%)
Ciclesonide Concentration(μM)
E
Cyc 5μM
SAG 50nM
SAG 1μM
DMSO
Bud
F
Relative Smo::EGFP Cilial Intensity (Ctl%)
Cyc 5μM + Bud Gradient
SAG 50nM + Bud Gradient
SAG 1μM + Bud Gradient
Bud Concentration(μM)
G
Relative Top-Flash Signal (Fold/Ctl%)
Bud Gradient
Wnt3a + Bud Gradient
Wnt3a Primed by Bud Gradient
Bud Concentration(μM)

Fig.S5

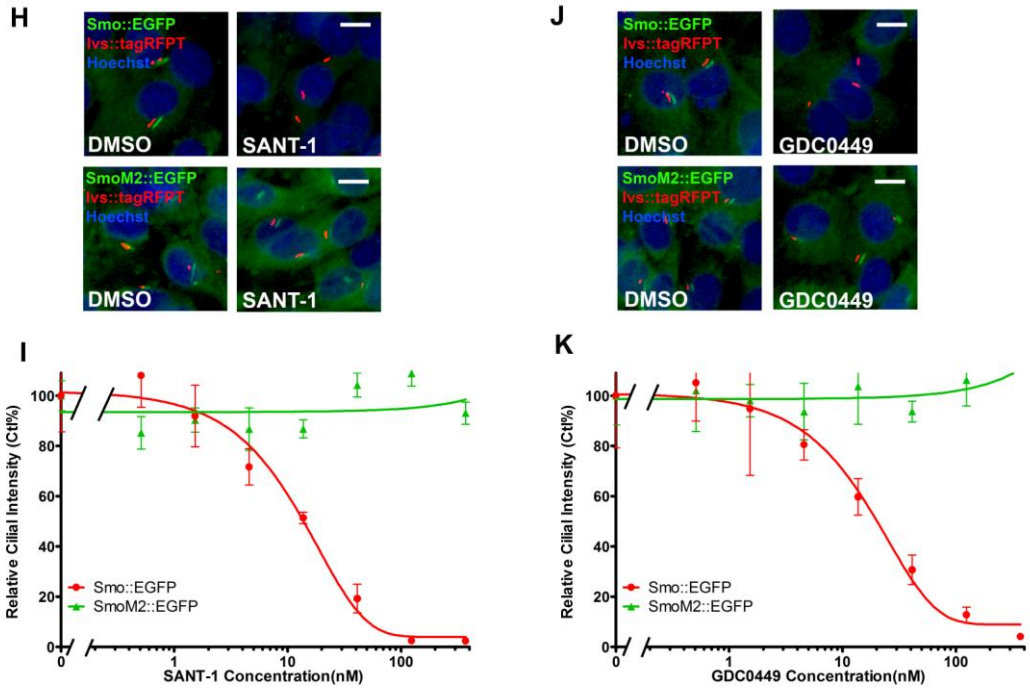

Fig. S5 (Continued)

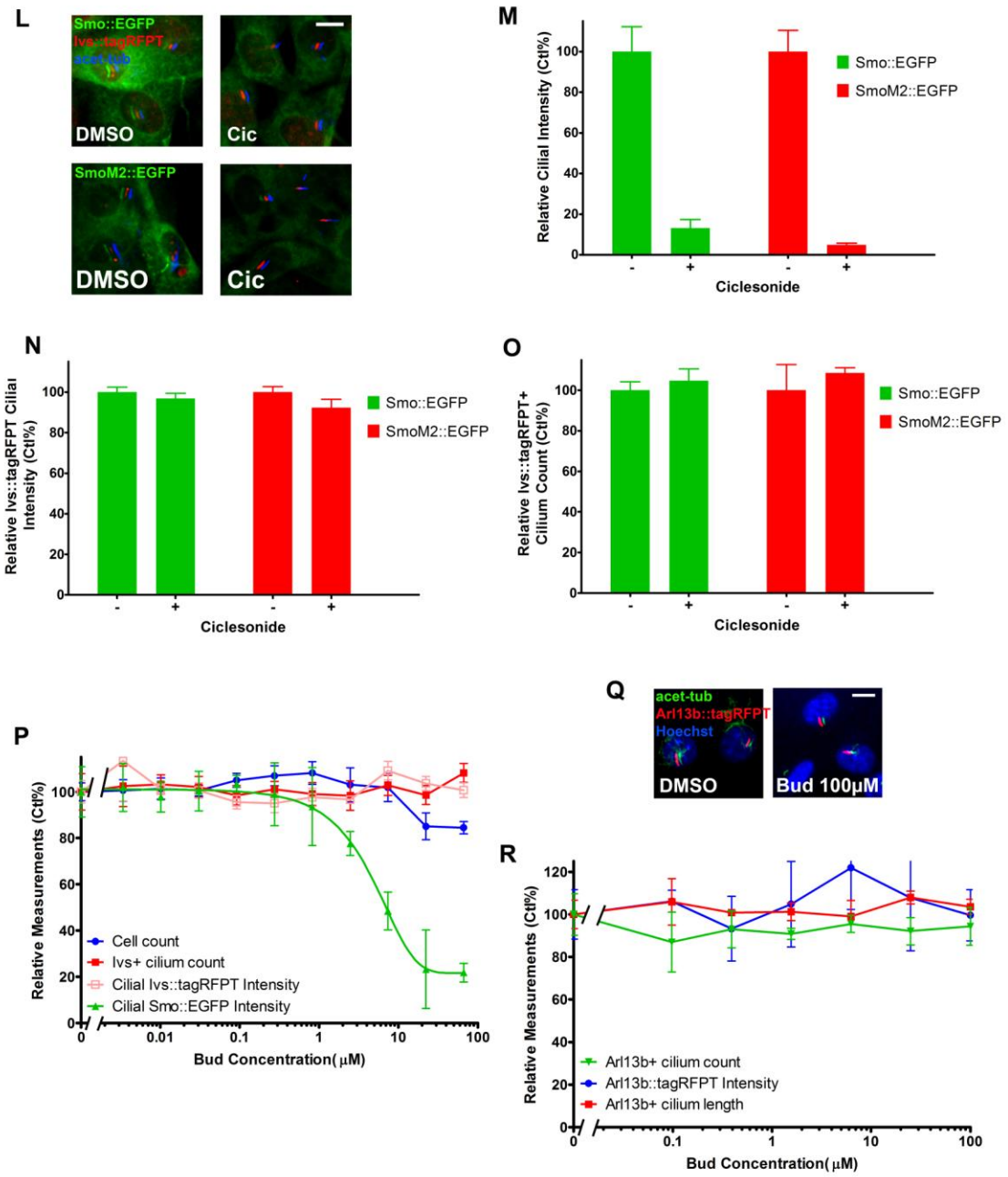

Fig. S5 (Continued)

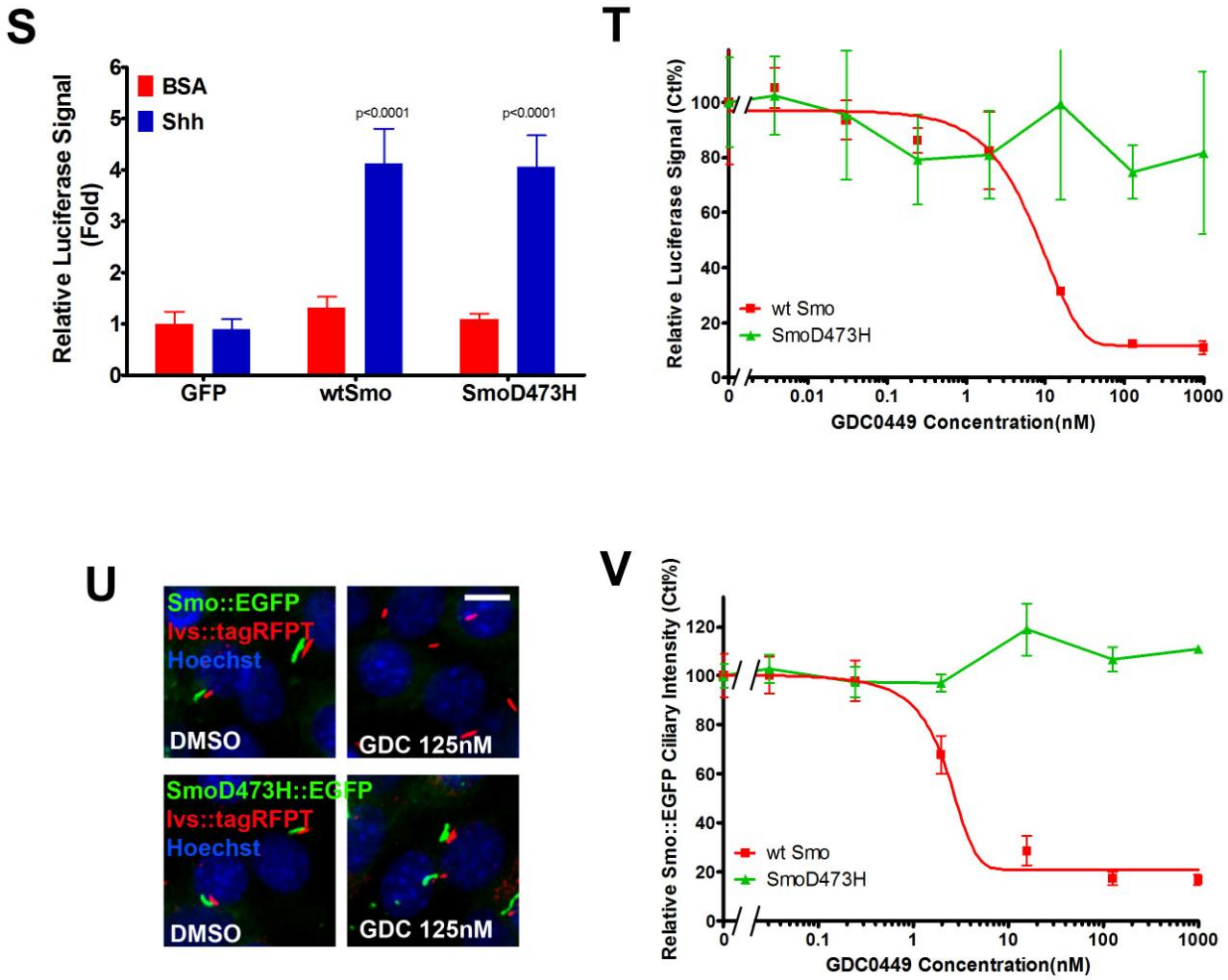

Fig. S5 (Continued)